The Dissertation Committee for Sabin Kshattry Certifies that this is the approved version of the following Dissertation

Human enzyme depletion of cyst(e)ine for pancreatic cancer therapy

Committee:

John DiGiovanni, Supervisor

George Georgiou

Everett M. Stone

Stefano Tiziani

Human enzyme depletion of cyst(e)ine for pancreatic cancer therapy

by

Sabin Kshattry

Dissertation

Presented to the Faculty of the Graduate School of

The University of Texas at Austin

in Partial Fulfillment

of the Requirements

for the Degree of

Doctor of Philosophy

The University of Texas at Austin

May 2018

Dedication

To my mother for constantly pushing me to achieve new heights; without your pushing, I would still be in your womb.

To my father for teaching me that the pursuit of knowledge is not a means towards an end but an end in itself.

To my brother, my greatest confidant, for having such an unwavering belief in me, which I myself sometimes lack.

Acknowledgements

I would like to first thank Dr. Randall Goldblum and Dr. Karen Browning, directors of the UT Austin arm of the UTMB-UT Austin MD-PhD program, for taking a chance on me. To have worked as hard as I did in undergrad only to get two interviews from MD-PhD programs and then get waitlisted from both of them, your decision to accept me came at a time when I was at a very low point and my faith in the "American Dream" was being tested on a daily basis. You decided to look past my status as an international student and put your faith in my potential, for which I will be forever grateful. I thank you for giving me the opportunity to start this journey and for your support throughout.

I would like to thank my advisor Dr. John DiGiovanni for his endless support and for giving me considerable flexibility to explore new directions in my project, which was very empowering and has played a crucial role in my development as an independent researcher. I would also like to thank Dr. Stefano Tiziani and his graduate student Paul Gries for allowing me to use the GC-MS instrument and teaching me the technical details of proper usage. The metabolomics aspects of my project, which is a significant portion, would not have been possible without their support. I am grateful to Dr. Yue Li for her crucial assistance with flow cytometry and confocal microscopy. I would also like to express my gratitude to my other committee members, Drs. George Georgiou and Everett Stone for their advice and encouragement.

I am tremendously thankful to all the members of the Digiovanni lab, past and present. Dr. Achinto Saha has almost been a second mentor to me answering my endless questions – I thank you for your patience and guidance. The day-to-day drudgery of

graduate school and the toll taken by all the failed experiments on one's psychological well-being is hard to overcome without having an amicable group of people in the lab to share those experiences with. I thank Zhao Chen, Steve Carbajal, Lisa Tremmel, Fernando Eguiarte, Songyoen Ahn, Dr. Okkyung Rho, Carly Wilder, Jeremy Cheng, Dr. Jiyoon Cho and Dr. Jaya Srivastava for indulging with me in my eccentric mannerisms and sharing with me yours. I hope someone will carry on the yet-to-be-proud tradition of "Fancy Fridays."

I appreciate the companionship that I have received from all my friends, near and far. Even just speaking on the phone with all of you is a huge stress reliever and helps me get through the day.

And finally, I want to thank my family who has helped me keep my sanity throughout this constant battle this is graduate school. Everything that I do is for you; everything that I am is because of you. School has kept me away for quite some time now, but I cannot wait to be back home soon. I love you.

Abstract

Human enzyme depletion of cyst(e)ine for pancreatic cancer therapy

Sabin Kshattry, Ph.D.

The University of Texas at Austin, 2018

Supervisor: John DiGiovanni

Pancreatic ductal adenocarcinoma (PDAC) has a dismal 5-year survival rate at 8%. Since targeting *KRAS*, the driver oncogene in PDAC, has not been a clinically successful endeavor to date and given that the growth of pancreatic tumors is intricately linked to reactive oxygen species (ROS) detoxification mechanisms, perturbation of oxidative balance might be an effective therapeutic strategy. A major intracellular antioxidant is glutathione (GSH), a tripeptide made of glycine, glutamate and cysteine. Cysteine (L-Cys), which has the functional moiety of GSH, can either be synthesized *de novo* intracellularly or imported, predominantly as cystine (CSSC) that is reduced intracellularly to L-Cys. Recently, our group has engineered a human enzyme called cyst(e)inase that degrades both extracellular L-Cys and CSSC and is a safe and effective therapeutic agent for multiple cancer models.

In our study with three pancreatic cancer cell lines, we found that even though cyst(e)inase depleted intracellular L-Cys and GSH in all three, only one "sensitive" cell line exhibited ROS accumulation and apoptotic cell death; the other two "resistant" cell

lines were able to arrest their growth and maintain survival. Further mechanistic exploration showed that only the resistant cell lines were capable of maintaining mitochondrial fitness during L-Cys/CSSC depletion. Since resistance seemed predicated on maintenance of functional mitochondria, a major ROS producer, we sought to sensitize the resistant cells to cyst(e)inase by concurrently inhibiting other antioxidant pathways. As expected, this approach led to synergistic inhibition of cell survival in all three cell lines with the most striking effect and high translational potential provided by auranofin, a thioredoxin reductase inhibitor and an approved drug for rheumatoid arthritis. Treatment of cyst(e)inase and auranofin in combination caused a synergistic increase in mitochondrial ROS and apoptosis, and also led to inhibition of mitophagy – a cellular mechanism for mitochondrial quality control. Treatment of nude mice harboring pancreatic cancer xenografts recapitulated these results: auranofin sensitized the completely resistant cell line to cyst(e)inase without causing any systemic toxicity. Our data provides strong rationale to investigate the efficacy of cyst(e)inase and auranofin combination to treat patients with PDAC.

Table of Contents

List of Figures

List of Illustrations

Chapter 1: Introduction

1.1 Background: Pancreatic cancer and its vulnerabilities

Pancreatic ductal adenocarcinoma (PDAC) is a deadly disease that continues to have a very low 5-year survival rate (8%) despite our increased understanding of the underlying cancer biology and improved ability to perform complex surgical procedures[1,2]. One major reason for this is that over 80% of patients present at a stage when surgical resection is no longer possible. They are then at the mercy of chemotherapy, most of which provide a median survival increase of about half a year and are associated with many toxicities[2]. To improve survival and quality of life for PDAC patients, new agents that are more effective and less toxic need to be discovered.

One of the most defining features of pancreatic adenocarcinoma is activating mutations (>90%) in the *KRAS* gene[3], which is thought to be the major oncogenic driver with subsequent mutations in other tumor suppressors serving as bottlenecks for tumor progression to adenocarcinoma. Genetically engineered mouse models also show a similar genetic progression providing a platform to more accurately study this phenomenon[4]. Mounting evidence suggests that the major oncogenic mutation in the Kras protein in pancreatic cancer is a substitution at the 12th position from a glycine to aspartate ($Kras^{G12D}$). More recently, knock-in models and doxycycline induced silencing of *KRAS* in genetically engineered mouse models have uncovered crucial dependencies – loss of *KRAS* expression resulted in arrested proliferation and rapid tumor regression in these

models[5,6]. Although *KRAS* extinction *in vitro* and in genetic mouse models can inhibit growth of human PDAC cell lines in some contexts, clinical efforts at targeting downstream components of RAS-MAPK (mitogen activated protein kinase) pathway have not been very successful to date. Furthermore, some have even reported a subset of pancreatic cancer cells that are resistant to *KRAS* ablation, and are in fact, more tumorigenic due to the presence of stem-like features[7,8]. Hence, identifying other vulnerable pathways in pancreatic cancer might provide a more effective therapeutic approach.

1.2 Metabolic requirements of cell proliferation

Unicellular organisms face intense evolutionary pressure to assimilate available nutrients into biomass and proliferate as quickly as possible. They have evolved their metabolic machinery to direct available carbon, nitrogen and free energy into pathways that lead to the production of a new cell. On the other hand, when nutrients become scarce, they need to extract the maximum possible free energy from available resources to maintain survival[9]. This dichotomy can be conceptualized with a real-world human example. Suppose, a tribal person who is living in the forest has access to some wood and is faced with the decision of how to make the best use of this resource. If he is facing this situation during the summer when vegetation is plentiful and food is readily available, he might use this wood to make a house for shelter, and even make an encircling fence (biomass accumulation). However, if he arrives at this decisional crossroad during the winter time when preservation of body heat becomes an extra survival task, and the scarcity of vegetation necessitates a more hunting-based diet, he might decide to use most of the wood

for making fire (energy generation). Similarly, the decision faced by unicellular as well as mammalian cells to whether proliferate or maintain survival imposes the need to channel available substrates through distinct metabolic routes. Consequently, regulatory mechanisms have evolved in organisms spanning almost all branches of life to control cellular metabolism as a function of nutrient availability which, in turn, guides the decision to whether proliferate or not[10].

In multicellular organisms, most cells have a constant access to nutrients and are therefore not limited by nutrient availability for proliferation. In fact, survival of the organism is dependent upon prevention of unrestrained proliferation of individual cells. This is ensured by mammalian cells through signaling mechanisms that allow uptake of nutrients and subsequent intracellular utilization only when instructed to do so by growth factors. Cancer cells overcome this dependence on growth factor signaling through genetic mutations which allows them uptake nutrients, particularly glucose and glutamine, and orchestrate their metabolism in a manner that is conducive to proliferation.

1.2.1 The Warburg Effect: Implications in cellular anabolism

The propensity of proliferating cells to metabolize glucose primarily through fermentation and excrete ethanol was first observed in yeast. Otto Warburg extended these observations to cancer cells and discovered that majority of the glucose carbon taken up by cancer cells is metabolized into lactate even in the presence of ample oxygen. This “aerobic glycolysis” seen in cancer cells, now famously known as the Warburg Effect, led Warburg to hypothesize that all cancers have dysfunctional mitochondrial. The Warburg Effect still

remains one of the most enduring hallmarks of cancer metabolism, which has found clinical application in ^{18}F-deoxyglucose positron emission tomography (FDG-PET) imaging. However, advances in cancer metabolism research over the last two decades and the concomitant, piling evidence that points to the importance of mitochondrial metabolism has made Warburg's hypothesis of cancer cells harboring damaged mitochondria untenable[11].

The presence of oxygen promotes normal, non-proliferating cells (where most of our current understanding of metabolic pathways is derived from) to maximize their adenosine triphosphate (ATP) yield by completely oxidizing glucose-derived pyruvate to carbon dioxide in the mitochondria via the tricarboxylic acid (TCA) cycle and oxidative phosphorylation. The fact that metabolism of a large portion of available glucose into lactate, which yields a net of 2 ATP molecules compared to the maximum of 36 ATP molecules produced by oxidative phosphorylation, can sustain the bioenergetic demands of proliferation in unicellular as well as mammalian cells implies that ATP availability is not a limiting factor for proliferation. ATP production is only a problem when resources are scarce, which is not a problem for mammalian cells as aforementioned. Moreover, complete oxidation of glucose carbon into CO_2 runs counter to the need of a proliferating cell for biomass accumulation. Recent work has slowly caused a paradigm shift in the field which has increased the appreciation for the Warburg Effect as an effective mechanism to support macromolecular biosynthesis rather than viewing it as an inefficient mechanism for ATP production[9,11,12].

Indeed, upstream metabolites of glycolysis can be shunted to important biosynthetic pathways. By re-routing glucose-6-phosphate into the pentose phosphate pathway, cancer cells can synthesize ribose-5-phosphate, which can subsequently be used for nucleotide synthesis. In addition, this diversion of glucose also results in the production of NADPH, which is very important for cells to maintain redox homeostasis (to be discussed later). Specifically in pancreatic cancer cells, oncogenic Kras has been shown to promote tumor maintenance by complementing the increased glycolysis with channeling of glucose substrates into hexosamine biosynthetic pathway for protein and lipid glycosylation, and the non-oxidative arm of the pentose phosphate pathway for nucleotide synthesis[6]. Upregulation of a specific enzyme phosphoglycerate dehydrogenase (PHGDH) allows the diversion of glyceraldehyde-3-phosphate towards the serine synthesis pathway, which is required for the maintenance of breast as well as lung cancer cells due to this pathway's pleitropic roles in nucleotide, amino acid and redox metabolism[13-15]. Another notable enzyme in the glycolytic highway is pyruvate kinase, which catalyzes the conversion of phosphoenolpyruvate (PEP) into pyruvate with concomitant generation of ATP from ADP. Proliferating cells almost universally express the M2 isoform of pyruvate kinase (PKM2), which is less active than the normal M1 variant that is present in most adult differentiated tissues. This might seem paradoxical at first glance, but the lower enzymatic activity actually allows for the accumulation of upstream intermediates which can serve as biosynthetic precursors. The tumor-promoting effects of this "bottleneck" at PKM2 is validated by the fact that either expressing the PKM1 isoform or using small molecule activators of PKM2 suppresses tumor growth[16].

1.2.2 Mitochondrial metabolism in cancer

Evidence against Warburg's original hypothesis started to surface as early as the 1950s showing that mitochondria in tumors and normal cells show similar oxidative capacity[17,18]. Fast-forward more than sixty years to present date, the diverse, established functions of the mitochondria for supporting cell proliferation seem as indispensable to tumor maintenance as it is to any discussion of tumor biology. Technological advancements have allowed us to actually quantify the oxidation of not just glucose but other substrates such as lactate in intact tumors in mice as well as humans[19-21].

The bioenergetic and biosynthetic functions of aerobic glycolysis are still not enough to satisfy a proliferating cell's demand for proteins, nucleotides and fatty acids[22]. Many of the precursors to these macromolecules are derived from mitochondrial TCA cycle (Krebs cycle), which can utilize multiple carbon sources such as glucose-derived pyruvate, amino acids such as glutamine and fatty acids to fuel ATP synthesis as well as synthesis of macromolecular precursors. For example, the TCA cycle intermediate citrate, which is formed through condensation of oxaloacetate and acetyl-CoA by the exclusively mitochondrial enzyme citrate synthase, can be exported back into the cytosol and cleaved by ATP citrate lyase (ACL) to re-generate acetyl-CoA in the cytosol that can then fuel fatty acid synthesis. Inhibition of fatty acid synthesis either by inhibiting ACL or acetyl-CoA carboxylase (ACC), which mediates the first committed step for fatty acid synthesis, suppresses tumor cell growth[23,24].

Oxaloacetate is another important metabolite that can be transaminated into aspartate by either the cytosolic (GOT1) or the mitochondrial (GOT2) aspartate

aminotransferase. Since a cell can synthesize aspartate as such, it is deemed a non-essential amino acid, and therefore even absent in some cell culture media formulations. However, since aspartate is indispensable for the synthesis of purines and pyrimidines, it is a requirement for cellular proliferation. As an amino acid, it is also a substrate for protein synthesis. In fact, a major function of the electron transport chain in proliferating cells is to support aspartate synthesis by maintaining the redox balance in the electron acceptor pool (i.e, NAD+)[25,26]. Growth arrest exhibited by cells that are defective in electron transport function can be rescued by supplementation with aspartate or by overexpression of the aspartate transporter[25]. Nucleotide and protein synthesis facilitated by aspartate is required for not only proliferation but also cell survival during stress conditions for the transcription of stress related genes and the translation of their protein products, which highlights the importance of aspartate in proliferative as well as quiescent metabolism. These observations provide a mechanistic link of how the increased reliance on oxidative phosphorylation during non-proliferative conditions[9] meets a cell's survival demand of energy production as well as basal nucleotide and protein synthesis.

The exit of precursor molecules (cataplerosis) from the TCA cycle needs to be carefully balanced by the entry of such intermediates into the cycle (anaplerosis) to maintain cycle function. The major anaplerotic precursor in proliferating cells is glutamine, which is oxidized in a step-wise fashion into the TCA cycle intermediate α-ketoglutarate that is eventually metabolized to oxaloacetate[27]. Thus, many cancer cells exhibit glutamine addiction, to overcome which they need to upregulate alternate forms of anaplerosis, most notably pyruvate carboxylation, which generates oxaloacetate via the carboxylation of

glucose-derived pyruvate[28,29]. Even though majority of cancer cells have intact mitochondrial function, small subsets of cancer cells harbor inactivating mutations in the mitochondrial enzymes fumarate hydratase and succinate dehydrogenase. Despite having a premature truncation of the TCA cycle, these cells are able to maintain a proliferative phenotype by fulfilling their biosynthetic needs either through pyruvate carboxylation[30,31] or through reductive carboxylation of α-ketoglutarate into citrate[32].

In the context of pancreatic cancer, a subset of cells that were able to survive *KRAS* extinction were surprisingly more tumorigenic due to the upregulation of genes involving mitochondrial function[7]. Moreover, pancreatic cancer cells have an augmented ability to maintain oxidative metabolism due to increased autophagic flux, a process through which the cell recycles intracellular nutrients as well as organelles such as mitochondria[33].

1.2.3 Integration of growth-factor signaling and altered metabolism

Activation of the PI3K/Akt signaling pathway is perhaps the most common genetic alteration in spontaneous human cancers. Activated PI3K/Akt causes increased glucose utilization by orchestrating a concerted program that features increased expression of glucose transporters as well as activation of glycolytic enzymes[11]. This oncogenic pathway also promotes glucose carbon flux into fatty acid synthesis by phosphorylating and activating ATP citrate lyase[24,34].

The well-characterized regulator of protein synthesis and cell growth, mechanistic target of rapamycin (mTORC1) is also downstream of Akt, and has many functions that are intertwined with metabolism including regulation of lipogenesis, autophagy, aerobic

glycolysis, pentose phosphate pathway, and *de novo* nucleotide synthesis[35]. Amino acids are essential for mTORC1 activation but mammalian cells have nutrient sensing mechanisms that allow mTORC1 to gauge the levels of not only amino acids but also glucose and oxygen[35] to send appropriate growth signals downstream. During starvation conditions, inhibition of mTORC1 is mediated through the integration of multiple inputs i.e., from AMPK via energetic stress and from GCN2 via amino acid deprivation[10,36].

The oncogenic transcription factor Myc, which is dysregulated in multiple cancers also has several important metabolic roles. It stimulates transcription of nuclearly encoded mitochondrial genes and leads to mitochondrial biogenesis[37]. It is also thought to mediate glutamine addiction in cancer cells through upregulation of glutaminase, which deaminates glutamine to glutamate[38].

As such, cancer and normal cells, more or less, possess the same metabolic network but they differ fundamentally in how they channel available resources into different pathways along that network to achieve distinct goals i.e., unbridled proliferation vs maximum energy generation. Glycolytic metabolism and mitochondrial substrate oxidation are both used to different ends by the two entities. This altered metabolism, now considered a core hallmark in cancer, lends itself to pursuits of drug development against targets that provide a wide enough therapeutic window. There are several analytical methods to study cancer metabolism – the one that we utilize in our studies will be discussed next.

1.2.4 ^{13}C tracer methods to study cancer metabolism

^{13}C tracer studies have gained prominence as one of the most frequently used modalities in metabolic research due, in part, to their ability to trace a wide varitey of metabolites in a single experiment not afforded by traditional ^{14}C tracer studies, which require purification, isolation, and carbon-by-carbon degradation of the metabolite of interest. ^{13}C is a stable isotope of carbon, which means that a wide variety of ^{13}C-enriched compounds are readily, commercially available. These compounds can be administered to metabolic entities (in our case, tumor cells) in the form of ^{13}C labeled nutrients (glucose and/or glutamine) and the ^{13}C distribution in different metabolites can be studied. In addition, the low natural abundance of ^{13}C (1.11%) minimizes confounding variables. Methods have been developed which even correct for the ^{13}C natural abuandance in such isotopic studies[39,40].

Mass isotopologue distribution (MID) analysis of metabolism is a method which studies ^{13}C enrichment in different metabolites through mass spectrometry (MS). It usually follows a chromatographic separation of the different metabolites through gas chromatography (GC) or high performance liquid chromatography (HPLC)[41]. GC/MS can elucidate crucial information about different metabolic pathways such as glycolysis, the TCA cycle, and non-essential amino acid synthesis, and hence provides a great avenue to study metabolism. The method is sensitive enough to detect a wide range of molecules in a cell. A gas chromatograph separates the various metabolites in a cell based on their differential interaction with the stationary and the mobile phase. As they elute off the GC column, they are bombarded through electron impact and broken up into specific ion fragments, which are detected by a mass analyzer and sorted according to their mass-to-charge (m/z) ratio. The ion fragment spectrum is unique for each molecule and serves as a

diagnostic tool. Hence, the different peaks on the GC spectrum can be assigned to specific metabolites by comparing their ion fragment spectrum with that of different molecules in a mass spectral library.

The extensive information about the different biochemical pathways that is available in the literature forms the basis for isotopologue analysis of metabolism. The known specifics of many metabolic reactions, which ranges from knowledge about the site of different reactions to the specific mechanisms that those reactions take, makes it easier to study the ^{13}C enrichment in the different metabolites which allows certain level of inference into the metabolic routes taken by those metabolites. In our context, the reactions of the TCA cycle are well characterized. Knowledge of carbon transfer through the cycle permits one to draw up a model showing the passage of ^{13}C label through the carbon backbone of different nutrients through the TCA cycle. (**Illustration 1.1**).

This model provides a good starting point for mass isotopologue analysis because it shows how the different isotopologues could be produced when different ^{13}C substrates are metabolized via distinct routes. For example, it shows how the labeling pattern in oxaloacetate is dependent on whether glucose or glutamine is labeled with ^{13}C, and whether glucose-derived pyruvate is oxidized to acetyl-CoA by pyruvate dehydrogenase (PDH) or carboxylated into oxaloacetate by pyruvate carboxylase (PC). If the cells are cultured in uniformly ^{13}C labeled glucose ([U-^{13}C]-glucose, glucose labeled in all six of its carbons), glycolysis produces pyruvate that is universally labeled. This pyruvate is transported to the mitochondria, where it has two fates. If it is metabolized via PDH, the resulting oxaloacetate pool will have an m+2 fraction (oxaloacetate ^{13}C-labeled in two of its carbons) and a lower m+4 fraction (produced if the same m+2 oxaloacetate molecule turns over 3 times in the TCA cycle – a rare event in cancer cells due to cataplerosis). On the other hand, if the ^{13}C labeled pyruvate is metabolized via PC, it will give rise to m+3

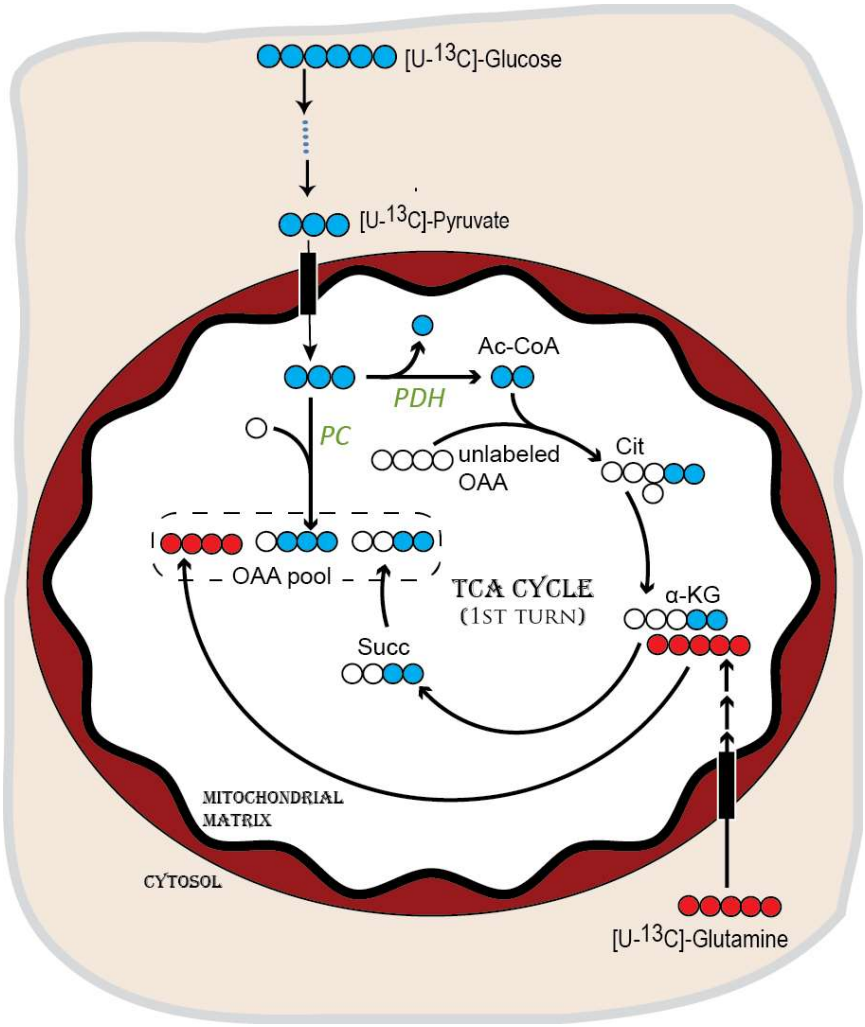

Illustration 1.1 Schematic showing the evolution of ^{13}C isotopologues of TCA cycle intermediates when glucose or glutamine is ^{13}C labeled.

Anaplerosis via [U-^{13}C]-glutamine is the major source of ^{13}C labeling in the oxaloacetate (OAA) pool. However, [U-^{13}C]-glucose-derived pyruvate also contributes to some labeling in OAA either via oxidation into acetyl-CoA (by pyruvate dehydrogenase, PDH) and subsequent entry into the TCA cycle or via carboxylation into OAA (by pyruvate carboxylase, PC). Abbreviations: Ac-CoA, acetyl-CoA; Cit, citrate; α-KG, α-ketoglutarate; Succ, succinate. Blue (glucose-derived) and red (glutamine-derived) circles represent ^{13}C labeled carbons.

isotopologue in the oxaloacetate pool. However, the largest fraction of isotopologue in oxaloacetate when the labeled substrate is glucose will be m+0 (unlabeled with ^{13}C) because most of the oxaloacetate in cancer cells is normally derived from anaplerosis through glutamine[27]. Consequently, if cells are cultured in [U-^{13}C]-glutamine, the major isotopologue in the oxaloacetate pool (and subsequently aspartate) will be m+4.

In our study, we will use this framework to conduct isotopologue analysis primarily with [U-^{13}C]-glucose as we explore the metabolic differences between different pancreatic cancer cell lines.

1.3 Opening a therapeutic window by perturbing oxidative balance

Cancer cells in general are known to have elevated production of reactive oxygen species (ROS). As aforementioned, a necessary requirement for proliferating cells is the synthesis of aspartate through the maintenance of a functional electron transport chain (ETC). Since majority of the ROS is produced by the ETC through incomplete transfer of electrons, cancer cells have a greater liability to combat toxic accumulation of ROS[42].

At moderate levels however, ROS actually promote tumorigenesis by inducing growth promoting pathways such as phosphorylation of MAPKs and extracellular signal-regulated kinase (ERK), and by inhibiting tumor suppressors such as phosphate and tensin homolog (PTEN) and protein tyrosine phosphatases[43-45]. Reactive oxygen species production has been shown to be a requirement for Kras-mediated tumorigenicity[46]. Specifically in pancreatic cancer, oxidative balance is maintained through Kras-mediated regulation of metabolic pathways[47] as well as through other upregulated mechanisms that control the levels of ROS[5,48].

These observations show how imperative it is for a cancer cell to maintain optimal levels of ROS since high levels are known to promote cell death. Cancer cells meticulously achieve this oxidative balance at a tumorigenic "happy" medium through the upregulation of antioxidant mechanisms[42]. Disrupting this balance potentially provides a unique therapeutic window for selective cancer killing in pancreatic cancer. Supporting this model, several studies have achieved selective killing of transformed cells through perturbation of redox status[49-51], which is further validated by the approved use As_2O_3 (Arsenic trioxide, Trisenox®) in the treatment of acute promyelocytic leukemia owing to its ability to inflict ROS-mediated cytotoxicity[52].

1.4 Cyst(e)ine depleting human enzyme

Glutathione (GSH), a tripeptide made of cysteine, glycine and glutamate, is one of the major intracellular antioxidants. In cancer, GSH metabolism is known to impart protection from apoptosis and induce multidrug as well as radiation resistance[53,54]. Thus, therapeutically disrupting GSH metabolism could be effective either as a monotherapy or in combination with other anticancer agents. Buthionine sulfoximine (BSO), which inhibits *de novo* GSH synthesis by inhibiting the rate-limiting enzyme (glutamate-cysteine ligase) has been used at the laboratory bench for long a time but has not yet been approved for use by the bedside possibly due to its toxic side effects[55]. Another feasible approach of decreasing glutathione synthesis is by depleting one of its three substrates. L-Cys, which contains the functional sulfhydryl moiety of glutathione, is readily synthesized by the transsulfuration pathway in many tissues including the pancreas[56]. As the precursor for

GSH biosynthesis, the pool of intracellular L-Cys plays a critical role in maintaining redox homeostasis. Due to an increased demand for GSH and protein synthesis, proliferating cells need to supplement endogenous L-Cys synthesis by importing it from the extracellular space, where majority of L-Cys is in its oxidized form cystine (CSSC), which is immediately converted to L-Cys upon import[57]. This excessive requirement of L-Cys/CSSC in cancer cells underlies our hypothesized selectivity factor afforded by our enzyme-mediated approach of depleting the extracellular cyst(e)ine (L-Cys and CSSC) pool.

Our group has recently engineered a human enzyme, known as cyst(e)inase, that degrades both extracellular L-Cys and CSSC[58]. The enzyme is made by mutagenizing a human enzyme from the transsulfuration pathway, cystathionine-γ-lyase (CGL), whose native substrate is cystathionine, but also has a very low L-Cys and CSSC degrading activity. The final mutagenized product shows a lower specificity for cystathionine, and increased specificity for L-Cys and CSSC (**Figure 1.1 a,b**). The fact that cyst(e)inase is derived by introducing only two amino acid substitutions from a fully human enzyme (CGL) will minimize its immunogenicity, a problem faced by bacterial enzymes used in human therapy. A single 50 mg/kg dose of cyst(e)inase administered intraperitoneally (i.p.) in mice was able to completely deplete serum CSSC for 3 days (**Figure 1.1 c**). Clinical success with the asparagine-depleting bacterial enzyme Oncaspar® in treatment of acute lymphoblastic leukemia (ALL) underscores the feasibility of this enzyme-based approach. Moreover, our previous studies with cyst(e)inase showing marked reduction of growth of multiple human cancers *in vivo* without any apparent toxicities[58] provides further rationale

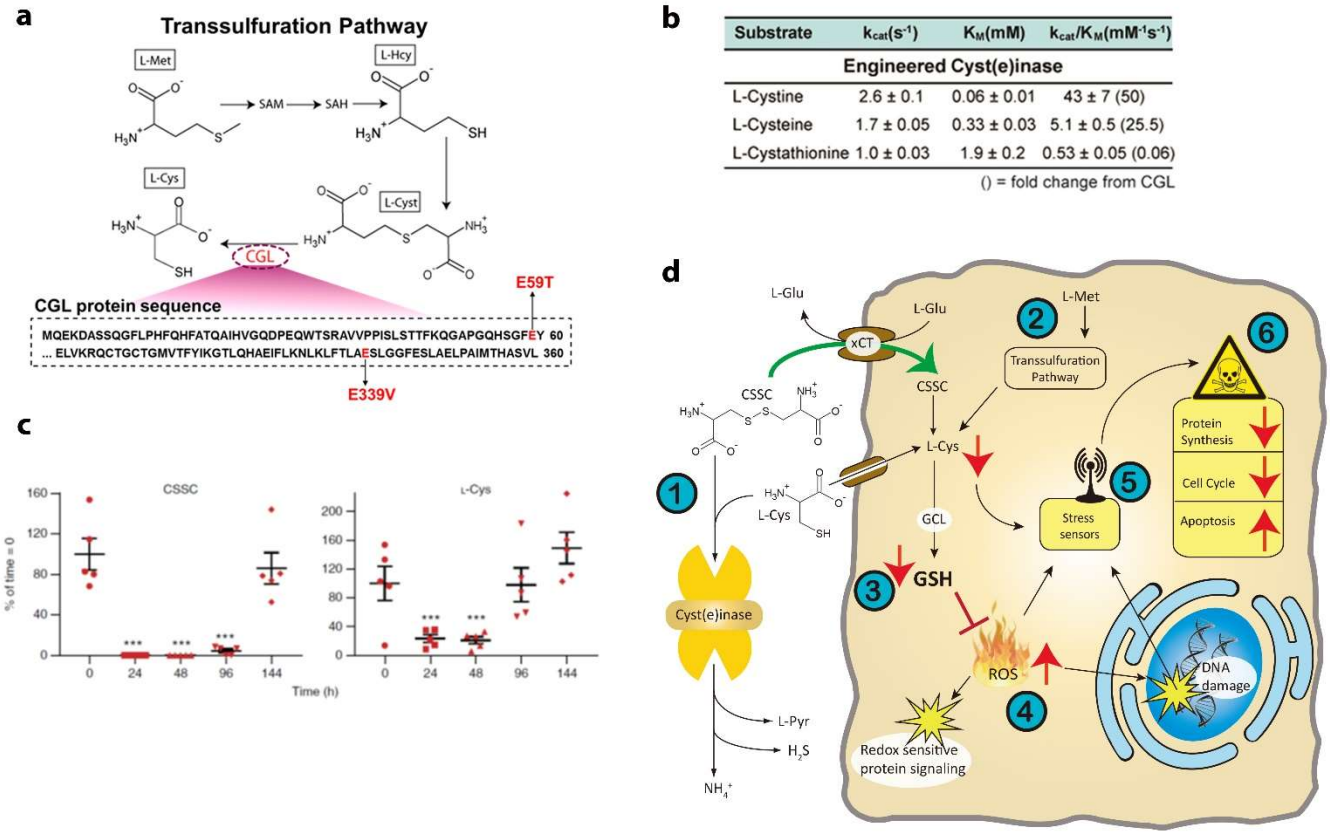

Figure 1.1 Cyst(e)inase is engineered to deplete extracellular CSSC and L-Cys.

(**a,b**) The human enzyme cystathionine-γ-lyase (CGL) from the transsulfuration pathway is mutagenized at the indicated amino acid residues (**a**) to increase its specificity for its non-native substrates, CSSC and L-Cys (**b**). (**c**) A single 50 mg/kg intraperitoneal (i.p.) dose of cyst(e)inase depleted CSSC (left) and L-Cys (right) in mouse serum for 3 days. (**d**) Cyst(e)inase degrades both L-Cys and CSSC in the extracellular space ①. Normal tissues can synthesize L-Cys through the transsulfuration pathway ②. It can also be imported via xCT from the extracellular space, where most of it is in the oxidized state as CSSC (green arrow). Many cancers need to supplement L-Cys synthesis with extracellular import to support increased demands of protein and GSH synthesis. Cyst(e)inase, by depleting L-Cys/CSSC from the serum, reduces intracellular L-Cys availability, which leads to reduced GSH synthesis ③. The resulting oxidative stress leads to DNA damage and perturbation of redox sensitive protein signaling pathways ④, which are sensed by various stress-sensing proteins ⑤ that then lead to the induction of multiple cytotoxic pathways ⑥. (**b**) and (**c**) were taken from (ref. [58]) with permission.

for the use of cyst(e)inase as a safe and effective cancer therapeutic option. We hypothesize that prolonged depletion of serum cyst(e)ine using cyst(e)inase will induce growth inhibitory and/or cytotoxic effects selectively in pancreatic cancer cells through a similar mechanism of action as observed in other cancer models[58] (**Figure 1.1 d**).

1.5 Drug combination analyses

Gemcitabine, a deoxycytidine analog that causes premature termination during DNA replication, has remained the standard-of-care for pancreatic cancer for about two decades even though it produces only a modest increase of survival of around half a year[59]. Given the complex interplay between many growth-promoting and survival pathways that contribute to pancreatic cancer's penchant for chemotherapeutic resistance, a better therapeutic strategy for combating this disease is by using multiple drugs in combination. While cyst(e)inase represents an excellent single-agent candidate for the treatment of many cancers including potentially pancreatic cancer, it is likely to be very useful in combination with other drugs as well.

There have been a few notable combination therapies for pancreatic cancer that have translated their bench-side potential into bed-side results. Nanoparticle albumin-bound (*nab*)-paclitaxel, an albumin-bound paclitaxel administered as a colloidal suspension, was found to potentiate the effects of gemcitabine by increasing the intratumoral concentration of gemcitabine in preclinical therapeutic trials[60]. Subsequently, a multicenter phase III clinical trial demonstrated the improved efficacy of this combination (8.5 months) compared to gemcitabine alone (6.7 months)[61]. The greatest

increase in survival in advanced PDAC to date has been achieved with FOLFIRINOX (a combination of folinic acid, 5-fluorouracil (5-FU), irinotecan and oxaliplatin) which increases survival to 11.1 months versus 6.8 months with gemcitabine; however, this highly toxic potpourri also has increased treatment-related toxicities, and is reserved only for patients with good performance [62].

In our study, we will test combinations of different drugs with cyst(e)inase for any potential additive or synergistic effects. Knowing the major mechanism through which cyst(e)ine depletion leads to growth arrest/apoptosis will allow us to rationally design combination treatments that produce synergistic effects. Exploring the optimal balance among synergistic growth inhibition, greater bioavailability, and minimal toxicity might lead us to a candidate combination that is the most feasible for clinical development.

1.5.1 Assessing synergy: Chou-Talalay method

A synergistic effect is when two drugs exert a more than an additive effect. Similarly, the effect is antagonistic when the combined drugs exert a less than additive effect. However, this raises the question as to what really constitutes as additive. It cannot be just an arithmetic sum of effects, which would imply that two drugs that exert an inhibitory effect of 50% and 60% respectively exert a combined inhibition of 110% - a physically impossible result. Synergy is a pharmacological phenomenon that is most frequently quantified using an isobologram.

Isobolograms can be constructed at different effect levels i.e., IC50, IC75 etc. To construct an IC50 (a concentration that inhibits cell survival 50% of control) isobologram, the IC50 values of each drug is determined individually (**Figure 1.2a**). These IC50 values

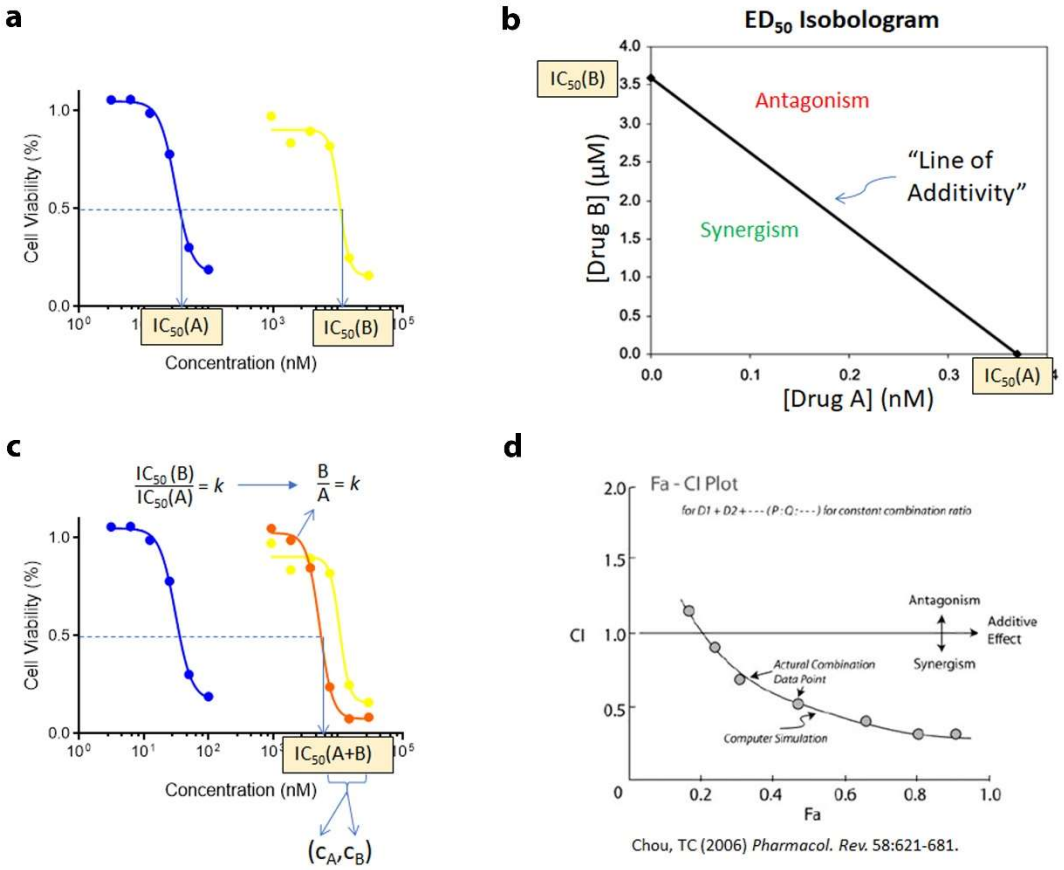

Figure 1.2 Quantifying drug interaction using the Chou-Talalay method.

(**a**) The IC50 values for two drugs A and B are determined individually. (**b**) These IC50 values make up the *x* and *y*-intercepts of the "line of additivity" on an IC50 (or ED50) isobologram. If combination treatment of A and B produces experimental points that fall below this line, then the drug combination is known to be synergistic; if the points fall above, the combination is antagonistic. (**c**) A constant-ratio drug combination experiment is performed by first calculating the ratio of the IC50s (denoted by *k*), and then combining the two drugs such that at every combination point, the ratio of doses is maintained at *k*. Since the IC50 value of the combination treatment represents a simple arithmetic sum of the two drug doses i.e., A+B = IC50(A+B), and also maintains the ratio B/A= *k*, the individual drug doses can be extracted from this IC50 value. These extracted doses plotted on the IC50 isobologram from (**b**) make up the "experimental point" for assessment of synergy/antagonism. (**d**) Alternately, a quantity called the Combination Index (CI) can be calculated for the drug combination at every experimental point using the computer software Compusyn. CI values less than 1 indicate synergy.

are plotted on the two axes and serve as the *x* and *y*-intercept for the straight line connecting these two points. Any experimental combination point that lies below this "line of additivity" is synergistic, anything that lies above is antagonistic (**Figure 1.2b**). Subsequently, a "constant-ratio" drug combination experiment between these two drugs is performed as follows. First, the ratio of the IC50 values of the two drugs is obtained – suppose it comes out to be 300. Then, the drugs are combined at different doses such that every combination point has this fixed ratio – usually, a high dose of each (e.g., ~IC95) is used to make the first combination dose and every dose thereafter is obtained via serial dilution. After treating cells with these combinations for the desired time period, the IC50 of the combination treatment is calculated (**Figure 1.2c**). This IC50 value is a sum of two drug concentrations, and when those individual drug concentrations are extrapolated, their ratio should be the same as the pre-determined ratio of individual IC50s (i.e., 300 in our example). Since there are two equations and two unknowns (the individual drug concentrations that make up the combination treatment's IC50 value), a complete set of linear equations can be written to extrapolate the individual drug concentrations as follows,

$$C_A + C_B = IC50_{AB}$$

$$C_B / C_A = 300$$

C_A and C_B are individual drug concentrations that are combined at a constant ratio and produce $IC50_{AB}$ in combination. The point formed by (C_A,C_B) is then plotted on the IC50 isobologram, which determines if this specific two drug combination is synergistic. Synergy/antagonism at other effect levels (i.e., IC25, IC75) can be assessed using this same concept.

On a similar note, to quantitatively assess the extent of drug interaction, a quantity called the combination index (CI) must be calculated using the following equation,

$$CI = \frac{C_{A,x}}{IC_{x,A}} + \frac{C_{B,x}}{IC_{x,B}}$$

$C_{A,x}$ and $C_{B,x}$ are the concentrations of drugs A and B used in combination to achieve x% effect. $IC_{x,A}$ and $IC_{x,B}$ are the concentrations of the same drugs used as single agents that achieve the same x% effect. CI values less than 1, equal to 1 and greater than 1 indicate synergy, additivity and antagonism, respectively. Chou and Talalay were the first to introduce these principles of studying drug interactions and methods to quantify them[63], which have now been adapted into a computer software called "Compusyn"[64] that can calculate CI values as a function of affected fraction of cells (Fa), which can then be used to determine whether the combinatorial effect produced by two drug concentrations is synergistic or not (**Figure 1.2d**).

Despite the convenience and popularity of the Chou-Talalay method, it has a few drawbacks. One, in this method, the concentration-effect curve (as shown in **Figure 1.1a**) is linearized by logarithmic transformation, a method which dates back to a period when investigators did not have access to nonlinear regression analytical tools and one that actually causes an underestimation of the steepness of the concentration-effect curves after transformation[65]. Secondly, this method requires well-established concentration-effect curves of the drugs as single agents[64], which is time-consuming and also not always available i.e., in experiments that use only a few concentrations of the combined drugs.

1.5.1 Assessing synergy: Bliss independence model

A viable, alternate method of quantifying drug interaction when dose-response curves are nonstandard or unavailable is using the Bliss independence model[66,67]. This model is derived from the complete additivity of probability theory[66], and it saves

experimental time and resources by obviating the need to generate concentration-effect curves for single agents before a combination experiment.

Suppose two drugs A and B are combined at concentrations *a* and *b*. If their individual inhibitory effect on cell/tumor growth (expressed as fraction affected relative to control) is I_a and I_b, respectively, the expected inhibitory effect of the combination can be calculated using the complete additivity of probability theory as

$$I_{ab,exp} = I_a + I_b - I_a \times I_b$$

The observed combined inhibitory effect, $I_{ab,obs}$ (derived from the actual drug combination experiment) is then compared with $I_{ab,exp}$ to make conclusions about the nature of drug interaction using the following decision chart.

$$I_{ab,obs} \begin{cases} > I_{ab,exp} & Synergy \\ = I_{ab,exp} & Independent \\ < I_{ab,exp} & Anatagonism \end{cases}$$

In addition, an isobologram plotting the $I_{ab,exp}$ and $I_{ab,obs}$ in the *x* and the *y* axis, respectively can be used to visually infer the extent of synergy achieved by two drugs as well as to compare the magnitude of synergy between multiple drug combinations in different cell lines[68] (**Figure 1.3**). This method is especially useful in high-throughput screening settings where a large dose range for multiple drugs becomes impractical, and in situations where the dose-response curves for single agents cannot be modeled by the standard four-parameter logistic nonlinear regression curves[66]. In our studies of drug combinations with cyst(e)inase, we will extensively use this method for assessing synergy.

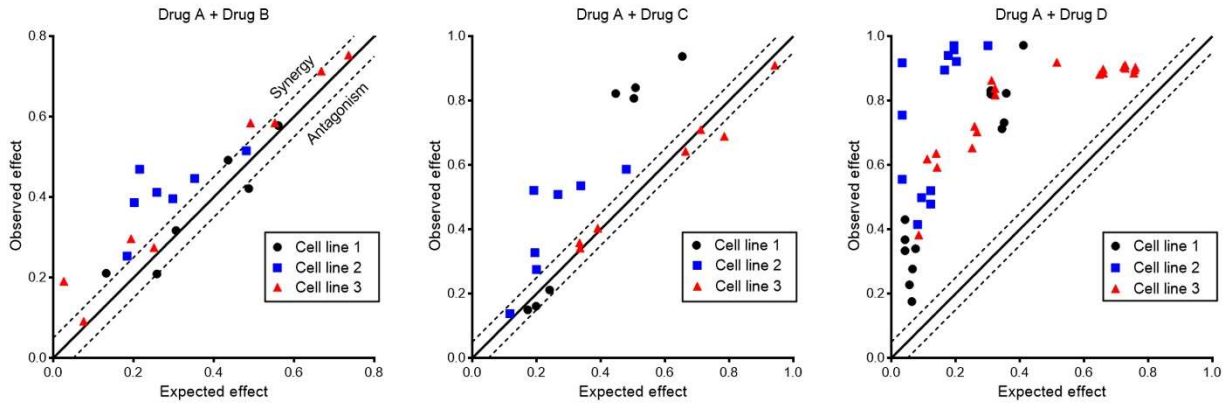

Figure 1.3 Assessing drug interaction using the Bliss model based isobologram

Plotting the observed effect (obtained from an actual combination experiment) versus the expected effect (calculated using the Bliss method) of a two-drug combination is a convenient method to assess the extent of drug interaction from multiple drug-combination experiments and to compare the effects of those combinations between different cell lines. Experimental data points that fall in the upper left region of the isobologram indicate increasing level of synergy.

1.6 Dissertation outline: Exploring the gamut from *in vitro* to *in vivo*

In our process of characterizing the efficacy of cyst(e)inase for pancreatic cancer therapy, we started our journey by exploring the effects of treatment *in vitro* in multiple pancreatic cancer cell lines. We used three pancreatic cancer cell lines, two of which had mutated *KRAS* (Panc1, $Kras^{G12D}$ and MIA-PaCa2, $Kras^{G12C}$) and one had wild-type (WT) *KRAS* (BxPC3). After observing that MIA-PaCa2 and BxPC3 were more resistant to cyst(e)ine depletion, we delved deeper into the mechanistic underpinnings behind this phenomenon through which we uncovered the survival mechanisms employed by these resistant cells. This allowed us to rationally design drug combinations that constituted of inhibiting those survival pathways while concurrently treating with cyst(e)inase, which led to our discovery of several synergistic candidates for further preclinical study. We then moved on to demonstrate that our lead combination candidate, which provided the best potential for clinical translation, was able to recapitulate its *in vitro* synergistic effects in xenograft mouse models without any signs of systemic toxicity.

1.6.1 Establishing the mechanism of action and cause for resistance

As expected, cyst(e)inase caused a near complete depletion of intracellular L-Cys and GSH in all three cell lines; however, ROS-mediated apoptosis was seen in only Panc1 cells. The other two "resistant" cell lines were able to halt proliferation and maintain survival under cyst(e)ine deprivation. As discussed earlier, when cells assume such a non-proliferative phenotype, they have an increased tendency to channel their substrates into mitochondrial oxidative phosphorylation. Therefore, we explored the differences in mitochondrial metabolism between these cell lines. During cyst(e)inase treatment, MIA-PaCa2 and BxPC3 were able to sustain anaplerosis of the TCA cycle for aspartate synthesis

as well as electron transport chain function for ATP synthesis, which were compromised in Panc1. This hinted towards the fact that the ability to maintain mitochondrial fitness during cyst(e)ine deprivation is the cause for resistance.

1.6.2 Rational design of drug combinations and isolation of lead candidate

We therefore inhibited mitochondrial metabolism at different nodes, which sensitized the resistant cells to cyst(e)inase treatment. Since inhibitors of mitochondrial metabolism are unlikely to offer a wide enough therapeutic window, we hypothesized that cyst(e)inase will synergize with concurrent inhibition of alternate antioxidant mechanisms because maintaining a functional mitochondrial machinery imposes a liability of detoxifying ROS produced by the electron transport chain. As expected, inhibitors of other antioxidant pathways synergized with cyst(e)inase among which auranofin, an inhibitor of thioredoxin reductase and an approved drug for the treatment of rheumatoid arthritis, stood out as a lead candidate for further *in vivo* work due to its extreme synergy with cyst(e)inase and its high translational potential in a combination therapy regimen.

1.6.3 *In vivo* validation

Cyst(e)inase treatment of nude mice bearing pancreatic cancer xenografts mirrored the *in vitro* sensitivity profile: Panc1 cells exhibited the greatest inhibition of tumor growth while BxPC3 were completely resistant. Combining auranofin and cyst(e)inase inhibited growth of MIA-PaCa2 and BxPC3 xenografts without causing any overt signs of systemic toxicity. Our results that we describe herein provide a strong rationale for the further clinical development of cyst(e)inase and auranofin combination in the treatment of pancreatic cancer.

Chapter 2: Materials and Methods[1]

2.1 Reagents

CB-839, Quercetin, Myricetin (Selleckchem); Glutathione ethyl ester, Buthionine sulfoximine, Curcumin (Sigma); Tigecycline, Rotenone, Oligomycin (Cayman); UK5099 (Tocris); Sulfasalazine (Fluka); Auranofin (Adipogen); L-aspartic acid 4-methyl ester hydrochloride (Alfa Aesar); Bafilomycin A1 (Sigma) were used. Ethaselen was kindly provided by Patrick Gunning from the University of Toronto.

2.2 Cell lines and culture

Human pancreatic cancer cell lines MIA-Paca2, Panc1 and BxPC3 were purchased from the American type culture collection (ATCC; Manassas, VA). Cell lines were confirmed to be mycoplasma free by PCR amplification (Applied Biological Materials Inc.) and 4,6-diamidino-2-phenylindole (DAPI) staining. Low passage cells (P<30) were cultured in either DMEM (MIA-PaCa2 and Panc1; Life Technologies) supplemented with 10% fetal bovine serum (FBS; Life Technologies) and 1% penicillin/streptomycin

[1]All chapters from this point are adapted from the following manuscript in preparation for publication:

Sabin Kshattry, Achinto Saha, Paul Gries, Stefano Tiziani, Everett Stone, George Georgiou, and John DiGiovanni. Cyst(e)ine depleting human enzyme combined with auranofin synergistically inhibits pancreatic cancer cell growth.

Author Contribtuions:
S.K., J.D. and G.G. wrote the manuscript. S.K. performed all the experiments with help and advice from A.S., and under supervision of G.G., E.S. and J.D. S.K., A.S., E.S., G.G. and J.D. interpreted the data. E.S. and G.G. provided the enzyme. P.G. provided critical help with sample extraction and measurements, and T.Z. provided reagents, instrumentation and expertise in metabolomics experiments.

(Pen/Strep; Life Technologies) or RPMI-1640 (BxPC3; Life Technologies) supplemented with 10% FBS, 1% Pen/Strep, 1 mM sodium pyruvate (Corning) and 1 mM HEPES (Sigma). All cells were cultured at 37 ºC in 95% air and 5% CO_2. Cystine deficient DMEM (Life Technologies, Cat. #21013024) and RPMI (Corning, Cat. #17104CI) were prepared by supplementing the base media with the aforementioned reagents and deficient nutrients except cystine.

2.3 Western Blotting

After treatment with indicated agents for the specified time, media was collected and centrifuged to pellet floating cells, and adherent cells were washed with PBS. Both cell fractions were combined and lysed in RIPA buffer with 1X protease and phosphatase inhibitor cocktails (Sigma). Protein concentration was quantified using DC Protein Assay (Bio-Rad) with bovine serum albumin (BSA) as a standard. Equal amounts of protein were separated on either fixed percentage or 4-15% gradient SDS-PAGE gels and transferred to 0.45 mm nitrocellulose membranes (Bio-Rad). After blocking in 3% bovine serum albumin (BSA) for 30 min, membranes were probed with specific primary antibodies (listed below) overnight at 4 ºC and secondary antibody at room temperature for 2 hours. Membranes were visualized with chemiluminescent detection kits (SuperSignal West Pico, Thermo Scientific for stronger protein targets; WesternBright Quantum, Advansta for weaker ones).

The following primary antibodies were used for western blotting: p-JNK$^{Thr183/Tyr185}$ (9251), PARP (9542), p-eIF2α^{Ser51} (3398), ATF4 (11815), p-p70S6K^{Thr389} (9234), p-S6

ribo$^{Ser235/236}$ (2211), S6 ribo (2217), p-Rb$^{Ser807/811}$ (8516), Rb (9309), Cyclin D3 (2936), cdc25C (4688), p-AMPK^{Thr172} (2531), AMPK (2532), xCT (12691), Thioredoxin 1 (2429), Thioredoxin reductase 1 (15140), Thioredoxin 2 (14907), Thioredoxin reductase 2 (12029), c-jun (9165), Cleaved caspase 3 (9664), Cleaved caspase 7 (9491), LC3B (3868), p62 (8025), Hexokinase II (2867), pyruvate dehydrogenase (2784) from Cell Signalling; Sestrin2 (sc-393195), Cyclin B1 (sc-752), Nrf2 (sc-13032), Cdk1 (sc-54), p27 (sc-776), succinate dehydrogenase-subunit A (sc-390381) from Santa Cruz Biotechnology; p-ATM^{Ser1981} (ab81292), GCL-C (ab53179) from Abcam; p-H2AX$^{Ser\ 139}$ (05-636, Millipore) and Actin (A5316, Sigma).

2.4 Mouse studies

For xenograft studies, one (MIA-PaCa2), two (BxPC3) or five (Panc1) million cells in a 200 μL solution of Matrigel (Corning) and serum free media (1:1) were injected subcutaneously into the hind flanks of 5-6 weeks-old athymic male nude mice (outbred homozygous *Foxn1^{nu}/ Foxn1^{nu}*; J:NU 007850, Jackson Laboratory). After tumor volumes reached a size of ~150 mm^3 (as calculated using the formula 0.5 x *l* x w^2, where *l* and *w* represent long and short diameters respectively, and are measured using a digital caliper), mice were divided into groups such that average tumor volumes in all the groups were approximately equal and treatment with indicated agents was begun as following: for single-agent cyst(e)inase studies, mice were given intraperitoneal (i.p.) injections twice a week with either 100 mg/kg cyst(e)inase or PBS. For combination studies, cyst(e)inase (50 or 100 mg/kg) was administered i.p. twice a week, and auranofin (3mg/kg) was

administered i.p. 3 times a week. Control mice were injected with PBS on cyst(e)inase treatment days and a 1:1 solution of 10% polyethylene glycol and 10% Tween80 in water (the solvent that was used to dilute 25 mg/mL DMSO-dissolved auranofin to make the 0.5 mg/mL auranofin solution used for treatment). Mice were given a semi-purified diet (AIN76A, 10 kcal%, Research Diets) and water *ad libitum*. Body weight and food consumption of mice were measured triweekly and weekly respectively. Experiments were terminated when tumor sizes in the control group reached their maximum limit as specified by an approved protocol from the University of Texas at Austin Institutional Animal Care and Use Committee (IACUC). At study termination, blood was collected via cardiac puncture following euthanasia and assessed for liver and kidney function by measuring serum levels of alanine aminotransferase and urea respectively using commercially available kits (Sigma).

2.5 Intracellular ROS measurement

Cells were seeded at a density of 1 x 10^5 (3.5-cm dish) or 5 x 10^5 (6-cm dish) and allowed to attach for ~24 hours. Following treatment with different agents for indicated times, 2',7'-Dichlorofluorescein diacetate (DCFDA, Sigma) for measuring total cellular ROS and MitoSOX Red mitochondrial superoxide indicator (Invitrogen) were added directly to the media at 20 μM and 2 μM final concentration respectively, and incubated at 37 ºC for 30 min. Cells were trypsizined, resuspended in PBS and data were acquired by flow cytometry (Guava easyCyte 8HT, EMD Millipore) and analyzed with FlowJo software.

2.6 Cell viability, cell growth and cell death assay

Cells were plated in 96-well plate at 5000 cells per well (100 µL). After ~24 h of attachment, cells were treated with 100 µL of different agents at 2X desired concentration for the indicated time points. At the end of treatment, media was aspirated and remaining viable cells were fixed with 10% formalin and stained with 0.05% crystal violet. After washing with water once, dye was extracted with 10% acetic acid and absorbance at 595 nm was measured. Relative cell viability was computed by comparing absorbance to untreated or vehicle-treated cells. Cell growth was assessed by crystal violet staining as well. Briefly, 10-20 x 10^3 cells were plated in 3.5-cm dish and allowed to attach for 1-2 days. At day = 0, one plate was stained with crystal violet as a surrogate measurement of cell number at the time of treatment. At every indicated subsequent time point, the relative cell number was calculated by measuring the fold change in crystal violet intensity relative to that at day = 0. Cell death was assessed by trypan blue exclusion test. Briefly, 2.5-5 x 10^5 cells were plated at day = -1, treated with different agents at desired concentration at day = 0 and trypsinized after indicated time of treatment. Dead/floating cells were also collected. A 1:1 mixture of trypan blue dye (Bio-Rad) and the cell suspension of interest was counted using a hemocytometer or TC20 Automated Cell Counter (Bio-Rad) for live and dead (blue) cell count.

2.7 Measurement of mitochondrial contents

1 x10^5 cells were plated in 3.5-cm dishes and allowed to attach for ~24h. Following treatment with different agents for 24 h, MitoTracker Green FM (for total mitochondrial

mass; Invitrogen) and MitoTracker Red CMXRos (for mitochondrial membrane potential; Invitrogen) were directly added to the media at 50 nM and 200 μM final concentration respectively. After incubation for 30 min at 37 ºC, cells were trypsinized and resuspended in PBS. Data were acquired by flow cytometry (Guava easyCyte 8HT, EMD Millipore) and analyzed with FlowJo software as previously described[69].

2.8 Intracellular glutathione measurement

Following treatment of 1 x10^5 cells for 24 h, media was aspirated, cells were washed with PBS, and pelleted and mixed with 150 μL of 5% sulfosalicylic acid (Sigma). Cells were lysed via 2 cycles of freeze-thaw, cell debris was pelleted by centrifugation and the glutathione content in the resulting supernatant was measured using a glutathione detection kit (Sigma). Separate dishes that were treated in parallel were used to quantify protein content, which was then used for glutathione normalization. Alternately, intracellular glutathione content was also measured in a 96-well format using the GSH/GSSG-Glo Assay (Promega) following a 24 h treatment with normalization performed to viable cell count.

2.9 Cell cycle analysis

After treatment of 5 x10^5 cells with different concentrations of cyst(e)inase for indicated time points, adherent and floating cells were harvested, washed with PBS and fixed in ice-cold 70% ethanol at 20 ºC for 2-4 days. After fixation, cells were washed, resuspended in Hank's Balanced salt solution (HBSS) containing RNase A (100 μg/mL;

ThermoScientific) and propidium iodide (PI; 40 µg/mL, Invitrogen) and incubated for 30 min at 37 ºC. Data of cell-cycle phase distribution was acquired by flow cytometry and analyzed by FlowJo software.

2.10 shRNA interference

shRNA constructs were purchased from Origene. The lentiviral transduction particles used for gene knockdown in target cells were generated in HEK 293T cells. Gene-specific shRNA plasmids are identified as follows:

Thioredoxin reductase 1 (TXNRD1):

shRNA #1: 5'-ACTATGACCTTATCATCATTGGAGGTGGC-3',

shRNA#2: 5'-AAGTCGAGGAGACAGTTAAGCATGATTGG-3'

Thioredoxin reductase 2 (TXNRD2):

shRNA #1: 5'- CAGGCGAAGTTACTCAAGGATTTGCTCTG-3',

shRNA#2: 5'- GACACCAGAAGTCTGAATTTGGAGAAGGC-3'

Infected cells were incubated in media containing puromycin (0.2-1 µg/mL) for at least 48 h before lysing cells for knockdown efficiency analysis or conducting further experiments. Puromycin was used for passaging knockdown cells but not during experiments with cyst(e)inase to avoid unforeseen combinatorial effects with puromycin. For double knockdown of *TXNRD1* and *TXNRD2*, cells that were stably transfected with *TXNRD2* shRNA #1 were infected with viral particles containing *TXNRD1* shRNA #2. Clones of cells harboring knockdown of both genes were obtained via multiple rounds of clonal selection and confirmation through western blotting.

2.11 Isobologram and evaluation of synergy

To evaluate synergism between two compounds we used the Bliss Independence Model as previously described[67],[68]. Briefly, the expected effect (E_{exp}) in a combination of two single agents is calculated from the effects of each separate agent as follows:

$$E_{exp} = E_{agent1} + E_{agent2} - (E_{agent1} \times E_{agent2})$$

The Bliss index of a combination is the ratio of the observed effect to the expected effect with values =1, <0, or >1 indicating additivity, antagonism and synergy respectively. Experimental data points that fall in the upper left region of an isobologram showing correlation of observed vs expected effects indicate increasing level of synergy.

2.12 Polar metabolite extraction and GC-MS analysis

Cells were plated in 6-cm (5 x10^5 cells) dishes and allowed to attach for ~24 h. After treatment with cyst(e)inase in regular media for indicated timepoints, media was aspirated and cells were washed twice with 0.9% saline solution. Polar metabolites were extracted and analyzed by GC-MS as previously described[30]. Cells were scraped in 500 µL of HPLC grade methanol:water (1:1) solution, transferred to a tube and snap frozen in liquid N_2 until further use. Cells were lysed via 3 cycles of freeze-thaw and cell debris was pelleted by centrifugation (14.8 x 10^3 rpm, 10 min, 4 ºC). The resulting supernatant was transferred to a glass vial, mixed with an equal volume of ice-cold chloroform, vortexed and centrifuged for polar-nonpolar phase separation. The top polar phase was transferred

to a new tube and dried using SpeecVac concentration. Metabolites were derivatized by incubation at 37 ºC for 1 h in 20 µL of methoxyamine hydrochloride (Sigma, 20 mg/mL dissolved in pyridine) then in 30 µL of *N*-methyl-*N*-(trimethylsilyl)trifluoroacetamide with 1% trimethylchlorosilane (Sigma) for another 1 h at 37 ºC. A small volume (0.2 µL) of derivatized samples were injected into a Thermo Scientific Trace 1310 gas chromatograph loaded with a Thermo TR-5 fused silica capillary column (length = 30 m, I.D. = 0.25 mm, film = 0.25 µm), which was connected to a Thermo ISQ single quadrupole mass spectrometer. Total ion current peaks of different metabolites were normalized to those of internal standard norvaline and isoleucine to control for differences in derivatization/injection and cell mass respectively.

2.13 [U-^{13}C]-glucose labeling

Glucose that is ^{13}C-labeled in all 6 carbons ([U-^{13}C]-glucose) was purchased from Cambridge Isotope Laboratories. For all ^{13}C labeling experiments, glucose and glutamine free DMEM (Life Technologies, Cat #A1443001) was supplemented with 25 mM [U-^{13}C]-glucose and 4 mM unlabeled glutamine, 10% dialyzed FBS and 1% Pen/Strep. Cells were plated at a density of 5 x 10^5 cells (6-cm dish) in regular media. After allowing ~24 hours for attachment, cells were treated with ^{13}C-labeled media containing either vehicle (10% glycerol in PBS) or cyst(e)inase. After 6 h of treatment, polar metabolites were extracted and analyzed using gas chromatography-mass spectrometry (GC-MS) as mentioned above. The abundance of the following ions was used for analysis of ^{13}C label incorporation: m/z 245–249 for fumarate, m/z 335–339 for malate and m/z 334–338 for aspartate. Mass

isotopologue distribution for each metabolite was corrected for natural abundance of ^{13}C using the software Metran[40].

2.14 Fluorescence microscopy for mitochondrial ROS

Cells were plated at a density of 3-5 x 10^3 in 8-well cell culture chamber slides and allowed to attach for ~24 hours. After treatment for indicated time, MitoTracker Green FM was directly added to the media at 50 nM final concentration to stain mitochondria 30 min prior to the following steps. Media was dumped into a waste jar as opposed to aspiration, which caused cells to detach. Cells were washed with PBS, the waste was dumped and any extra liquid on the slide was absorbed carefully using Kimwipes. A small volume of Vectashield mounting media containing DAPI (Vector Laboratories Inc.) was placed on each chamber and a glass cover slip was placed on top such that the media covered the entire chamber. Microscopy was performed with Olympus BX60 fluorescence microscope, and image acquisition was performed with the software DP Controller (Olympus).

2.15 mCherry-GFP-LC3

The plasmid (Addgene, plasmid #22418) was purified from E. coli and transfected into MIA-PaCa2 cells using Lipofectamine 3000 (Invitrogen). After 2-4 days, cells were incubated in media containing 1 μg/mL puromycin. Surviving cells expressing both green and red fluorescence were selected and expanded. Puromycin was used for passaging of transected cells but not during experiments. After treatment for indicated time, media was dumped, cells were washed with PBS, fixed with 4% paraformaldehyde solution and

washed again with PBS. A small volume of Vectashield mounting media containing DAPI was placed on each chamber and a glass cover slip was placed on top. Microscopy was performed with Leica TCS SP5 II confocal microscope, and image acquisition was performed with the software Leica Application Suite (Leica Microsystems).

2.16 Measurement of thioredoxin reductase activity

Total thioredoxin reductase activity was measured in 15 µg of protein sample using a Thioredoxin Reductase Assay kit (Cayman) according to the manufacturer's instructions.

2.17 Measurement of NAD+/NADH

Cells were plated in 96-well plate at 5000 cells per well (100 µL). After ~24 h of attachment, cells were treated with 100 µL of cyst(e)inase at 2X desired concentration for indicated time. At the end of treatment, NAD+/NADH was measured according to the NAD/NADH Glo Assay instructions provided by the manufacturer (Promega). Briefly, media was aspirated and replaced with 50 µL of PBS. Cells were lysed by adding 50 µL of 0.2 N NaOH with 1% Dodecyltrimethylammonium bromide (DTAB) and shaking for 5 min. 50 µL of this cell lysate was moved to a different well and treated with 25 µL of 0.4 N HCl (acidic conditions selectively degrade NADH). NAD+ is selectively degraded in the basic conditions of the original wells. Plate was incubated for 30 min at 60°C, allowed to equilibrate to room temperature and then neutralized with 25 µL of 0.5 M Tris base (acid-treated wells) or 50 µL of 1:1 HCl/Tris solution (0.5 M Tris + 0.4 N HCl, base-treated wells). 20 µL of this final solution was moved to a white-walled plate, mixed with 20 µL

NAD/NADH-Glo™ Detection Reagent, shaken for 2 h at room temperature and the luminescence was measured.

2.18 Statistical analyses

No statistical methods were used to predetermine sample size; selection of group sizes for animal experiments were driven by prior experience and literature precedence. The experiments were not randomized, and the investigators were not blinded during experiments or data analysis. Data are expressed as mean ± s.e.m. unless otherwise indicated and analyzed using GraphPad Prism 6. In xenograft experiments, outlier tumor values were identified and removed from all groups using the robust regression and outlier removal (ROUT) method with a 2% false discovery rate (FDR). Usage of the following statistical tests as applicable are described in figure legends: two-sided Student's *t*-test, one-way ANOVA and two-way repeated-measures ANOVA followed by Bonferroni's method for multiple-comparison test. Figure legends also describe the number of times experiments were repeated with similar results and the number of experiments that data is pooled from.

Chapter 3: Cyst(e)ine deprivation causes oxidative stress and apoptosis in sensitive cells but only growth arrest in resistant cells

3.1 Introduction

Following up on our work with cyst(e)inase in other cancer models[58], we decided to assess the efficacy of this human enzyme in pancreatic cancer cells. As discussed in **Chapter 1**, our rationale for using this approach is that cancer cells strike an intricate balance between ROS and antioxidants to support proliferation, and tipping the scale towards ROS accumulation can cause selective oxidative demise of cancer cells. In pancreatic cancer cells, cellular growth has been shown to be intimately linked with ROS detoxification mechanisms, which provides further justification for our line of attack. Herein, we describe our rather surprising finding that cyst(e)inase mediated depletion of intracellular L-Cys and GSH leads to oxidative stress and cytotoxicity in only one out of the three cell lines tested. We delve into the mechanistic details behind the cytotoxicity observed in the "sensitive" cell line and the inhibition of cell growth induced in the more "resistant" cell lines, and provide segue for the next chapter with an idea for exploring the nexus of resistance.

3.2 Results

3.2.1 Oxidative stress and cell death induced in only Panc1 cells

The three pancreatic cancer cell lines exhibited different levels of sensitivity to cyst(e)inase treatment (**Figure 3.1 a**) with Panc1 being the most sensitive while BxPC3 were most resistant. Cyst(e)inase was able to deplete intracellular cysteine to low steady-state levels in all cell lines (**Figure 3.1 b**) indicating that compensatory increase in *de novo*

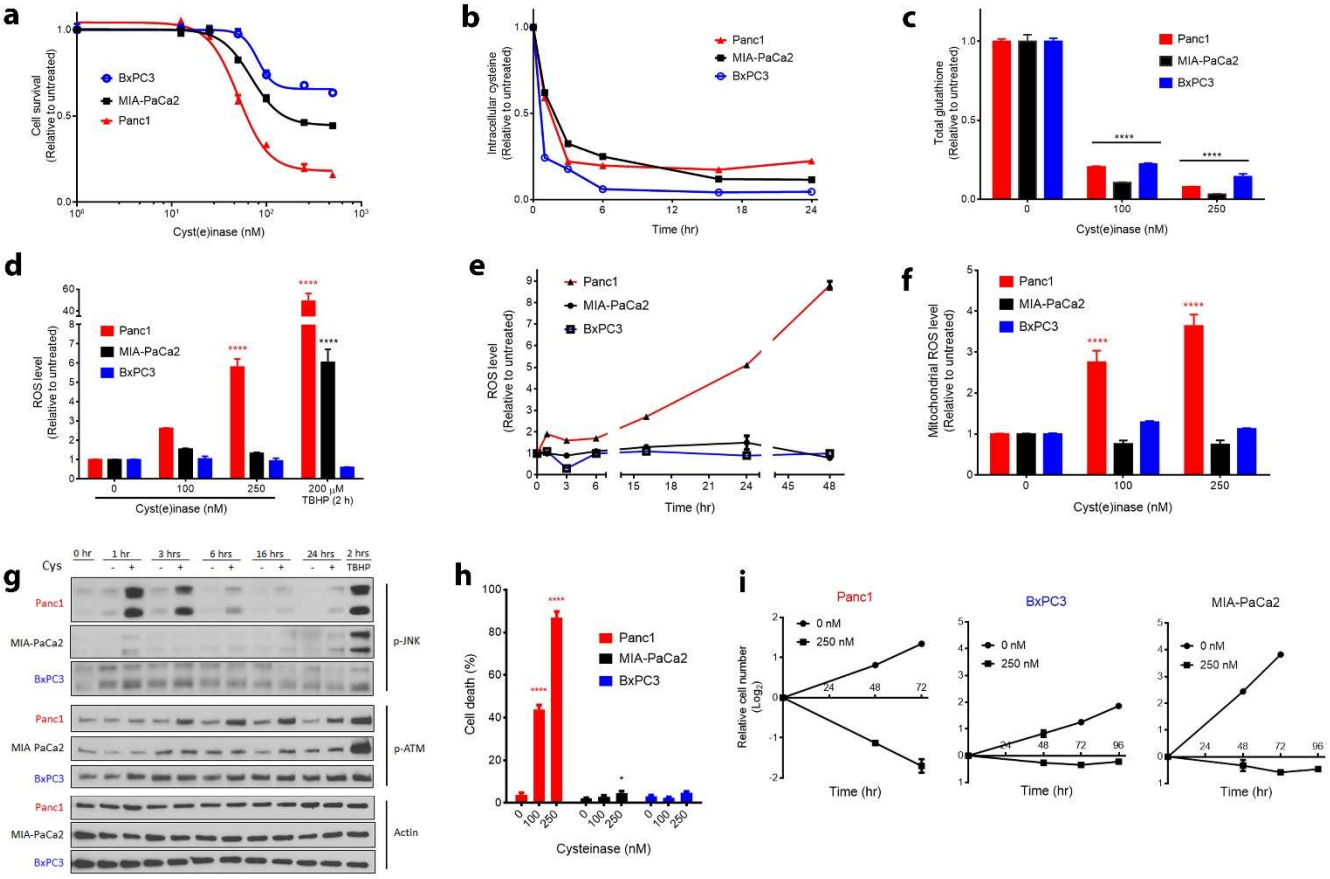

Figure 3.1 Cyst(e)inase causes oxidative stress and cell death in only Panc1 cells.

(**a**) Relative cell survival 48 h after cyst(e)inase treatment in 3 pancreatic cancer cell lines (n = 3 cultures for each dose). (**b**) Intracellular L-Cys levels upon treatment with 250 nM cyst(e)inase (one treated and one untreated culture for each time point, data from a representative experiment). (**c**) Intracellular GSH levels 24 h after treatment (n = 3 cultures for each dose). (**d,e**) Cellular ROS levels as assessed by 2',7'-dichlorofluorescin diacetate (DCFDA) fluorescence following a 24 h treatment (**d;** n = 3-5 independent experiments) and a 250 nM treatment (**e;** n = 3 technical replicates for each time point) with cyst(e)inase. *tert*-Butyl hydrogen peroxide (TBHP) treatment is included as a positive control for ROS accumulation (**d**). (**f**) Mitochondrial ROS levels as assessed by MitoSOX fluorescence following 24 h cyst(e)inase treatment (n = 3-6 independent experiments). (**g**) Oxidative stress signaling via JNK and ATM. Abbreviation: Cys, cyst(e)inase. (**h**) Cell death as assessed by trypan blue staining 48 h (Panc1) or 72 h (MIA-PaCa2 and BxPC3) after treatment (n = 3 independent experiments). (**i**) Cellular growth assay (n = 3 cultures for each time point). For **g**, "+" represents 250 nM cyst(e)inase treatment. All data represent mean ± s.e.m. except for **b.** *P < 0.05, ****P < 0.0001; compared to untreated controls; two-way ANOVA with Bonferroni's method for multiple-comparison test.

cysteine synthesis through the transsulfuration pathway probably does not account for resistance. As expected, cyst(e)inase mediated a complete depletion of intracellular GSH in all cell lines (**Figure 3.1 c**); however, only Panc1 cells exhibited accumulation of total cellular ROS (**Figure 3.1 d,e**) as well as mitochondrial superoxide (mitochondrial ROS, **Figure 3.1 f**). BxPC3 were particularly resistant to ROS accumulation as even *tert*-Butyl hydrogen peroxide (TBHP) treatment did not cause any oxidative stress (**Figure 3.1 d**). A known consequence of oxidative stress in pancreatic cancer cells is activating phosphorylation of c-Jun N-terminal kinase (JNK)[70], which was induced in Panc1 and MIA-PaCa2 cells by TBHP treatment but only in Panc1 cells by cyst(e)inase treatment (**Figure 3.1 g**). Another signaling event caused by ROS accumulation is through oxidative DNA damage, which activates the ataxia-telangiectasia mutated (ATM) protein kinase even in the absence of DNA double-strand breaks[71]. Again, activating phosphorylation in ATM was seen in only Panc1 cells after cyst(e)inase treatment (**Figure 3.1 g**). Downstream signaling through both of these stress-sensing kinases culminates in apoptotic cell death, which was corroborated by our finding that 250 nM cyst(e)inase caused more than 80% cell death in Panc1 within just 48 hours whereas no considerable cell death was seen in MIA-PaCa2 and BxPC3 cells (**Figure 3.1 h**). In fact, they were able to survive and maintain their cell mass even up till 96 hours of cyst(e)inase treatment (**Figure 3.1 i**). At initial glance, MIA-PaCa2 cells seem to be more sensitive to cyst(e)inase than BxPC3 (**Figure 3.1 a**); however, both of them do not exhibit cell death upon extended treatment. The method used to generate the cell viability curve in **Figure 3.1 a** i.e., relative to control, causes MIA-PaCa2 cells to "appear" sensitive due to its significantly higher rate of proliferation compared to BxPC3 (**Figure 3.1 i**). In fact, if inhibition of cell survival in MIA-PaCa2 cells were to be assessed 72 hours after cyst(e)inase treatment, the relative cell survival would be around 6% (~$1/2^4$ –approximated from **Figure 3.1 i**), a figure closer to

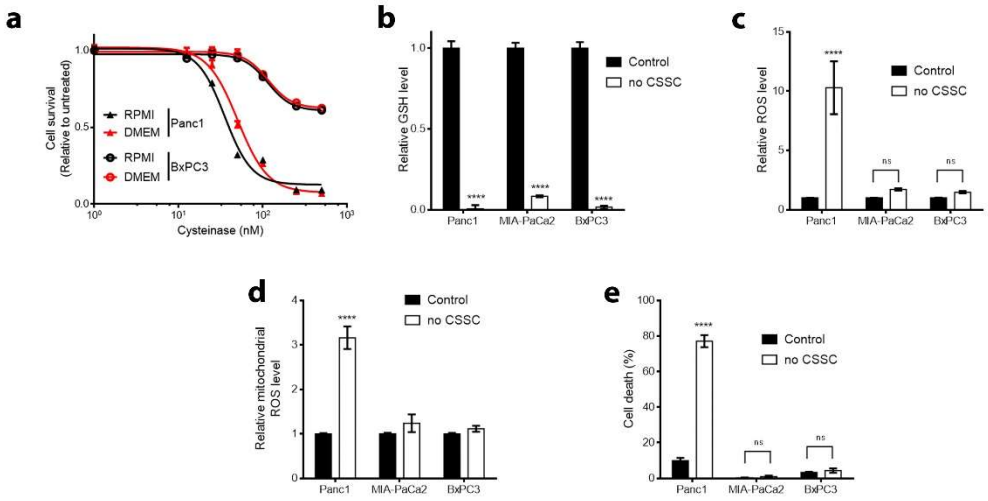

Figure 3.2 Cystine deficient media recapitulates effects of cyst(e)inase in pancreatic cancer cells.

(**a**) Relative cell survival of Panc1 and BxPC3 cells 48 h after cyst(e)inase treatment in indicated cell culture media ($n = 3$ cultures for each dose). (**b-d**) Intracellular GSH levels (**b**; $n = 3$ cultures), cellular ROS levels (**c**; $n = 4$ independent experiments), and mitochondrial ROS levels (**d**; $n = 3$ independent experiments) 24 h after treatment with indicated media conditions. (**e**) Cell death 48 h after treatment with indicated media conditions ($n = 2$ independent experiments). All data represent mean ± s.e.m. ****$P <$ 0.0001; compared to untreated controls; two-way ANOVA with Bonferroni's method for multiple-comparison test.

that of the sensitive Panc1 cells! However, since cyst(e)inase does not cause ROS accumulation and cell death in MIA-PaCa2 and BxPC3 cells, both of them will hereafter be considered cyst(e)inase resistant.

3.2.2 Cystine-deficient media recapitulates effects of cyst(e)inase

Since not all cell lines were cultured in the same type of medium (see Chapter 2.2), we wanted to investigate whether differences in culture medium played a role in determining sensitivity to cyst(e)inase. We found this not to be the case as Panc1 and BxPC3 did not change their sensitivity profile to cyst(e)inase treatment when cultured in the other cell line's default medium (**Figure 3.2 a**). Cystine-deficient medium however perfectly recapitulated the effects of cyst(e)inase treatment as it caused a complete depletion of intracellular GSH in all three cell lines (**Figure 3.2 b**), but increase in ROS (total cellular as well as mitochondrial) and cell death in only Panc1 cells.

3.2.3 Growth arrest in all cells and additionally apoptosis in Panc1

Recently, our group showed that cyst(e)inase induces cell cycle arrest at G_1 in multiple cancer models[58]. Specifically in pancreatic cancer cells, ROS is known to cause cell cycle arrest at the G_2/M checkpoint following JNK activation[70]. In agreement with these findings, Panc1 cells, in which cyst(e)inase caused ROS accumulation and JNK activation, initially exhibited a G_1 arrest (100nM) followed by a G_2/M arrest and an apoptotic sub-G_1 phase (250nM) after 24 hours of treatment (**Figure 3.3a**), whereas MIA-PaCa2 and BxPC3 underwent only a G_1 arrest (**Figure 3.3a**). Apoptotic signaling was initiated in Panc1 as early as 6 hours after cyst(e)inase treatment as evidenced by cleavage of poly (ADP-ribose) polymerase (PARP), which was expectedly absent from the other

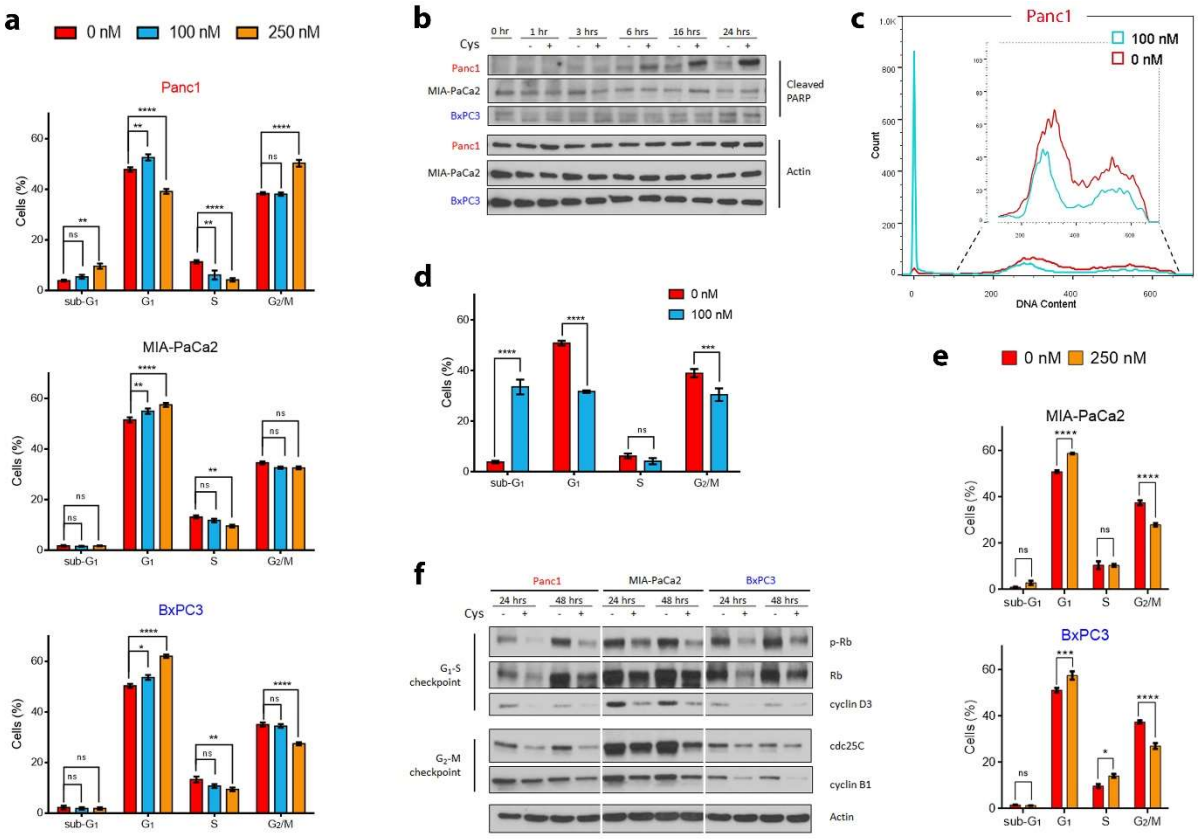

Figure 3.3 Cyst(e)inase induces cell cycle arrest in all cells but apoptosis in only Panc1 cells.

(**a**) Quantification of cell cycle phase distribution 24 h after cyst(e)inase treatment (n = 3 independent experiments). (**b**) Apoptosis signaling observed via cleavage of PARP following cyst(e)inase treatment. Abbreviation: Cys, cyst(e)inase. (**c-e**) Cell cycle phase distribution 48 h after cyst(e)inase treatment for Panc1 cells (**c**), and quantification of cell cycle phase distribution for Panc1 (**d**), MIA-PaCa2 and BxPC3 cells (**e**) 48 h after treatment (n = 3 independent experiments). (**f**) Regulatory cell cycle proteins following 24 and 48 h cyst(e)inase treatment. For **b** and **f**, "+" represents 250 nM cyst(e)inase treatment except for **f**, where "+" for Panc1-48 hrs represents 100 nM treatment. All data represent mean ± s.e.m. *P < 0.05, **P < 0.01, ***P < 0.001, ****P < 0.0001; compared to untreated controls; two-way ANOVA with Bonferroni's method for multiple-comparison test.

two cell lines (**Figure 3.3b**). At 48 hours, the apoptotic sub-G_1 phase in Panc1 cells accounted for 40% of cells even with the lower 100 nM treatment (**Figure3.3 c,d**) closely mirroring the magnitude of cell death seen in Panc1 cells when treated with that concentration for 48 hours (**Figure 3.1h**) indicating that apoptosis is the major mode of cell death caused by cyst(e)inase in sensitive cells. On the other hand, the two resistant cell lines still only exhibited only a G_1 arrest with a subsequent failure to reach G_2/M (**Figure3.3 e**), corroborating the absence of cell death in these cell lines (**Figure 3.1h**). Cell cycle proteins regulating the checkpoint for G_1-S transition and G_2-M transition decreased for all cell lines with treatment (**Figure3.3 f**).

3.2.4 Inhibition of mTORC1 signaling in all cells

Growth arrest following cyst(e)inase treatment could be a consequence of nutrient deprivation since L-Cys is also a substrate for protein synthesis. Mammalian cells have evolved two distinct amino acid sensing mechanisms – the mechanistic target of rapamycin complex 1 (mTORC1) signaling pathway is activated during amino acid replete conditions to stimulate protein synthesis while the general control nonderepressible 2 (GCN2) pathway is activated during amino acid starvation to inhibit protein translation. Specifically, GCN2, which is activated by uncharged tRNAs, links the deprivation of any single amino acid to inhibition of mTORC1[36]. Activated GCN2 phosphorylates eIF2α, which globally inhibits cap-dependent protein translation except for the translation of a few stress response transcription factors including ATF4, which transcriptionally upregulates Sestrin2. Sestrin2 inhibits the lysosomal localization of mTORC1, which is needed for its activation and subsequent phosphorylation of its downstream target p70S6K (**Figure 3.4a**). Cyst(e)inase treatment activated the eIF2α-ATF4-Sestrin2 axis (**Figure 3.4b**) and inhibited

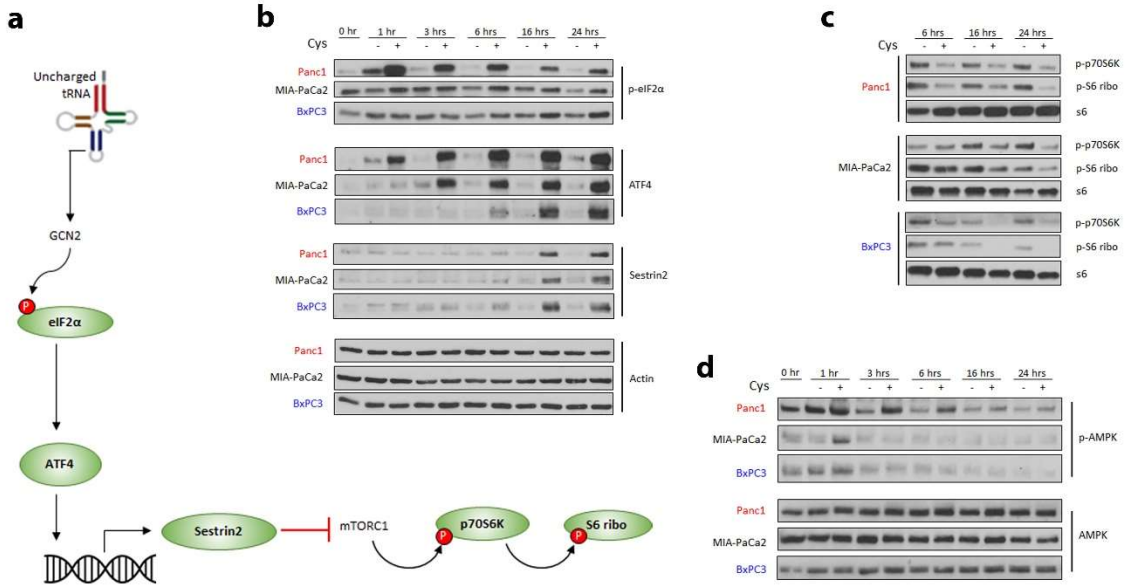

Figure 3.4 Inhibition of mTORC1 signaling through the eIF2α-ATF4-Sestrin2 axis.

(**a**) Schematic showing the pathway linking amino acid deprivation to inhibition of mTORC1 signaling. (**b,c**) Effect of cyst(e)inase (Cys) treatment on the eIF2α-ATF4-Sestrin2 pathway (**b**) and mTORC1 signaling (**c**) Effect of treatment on AMPK signaling. For **b**-**d**, "+" represents 250 nM cyst(e)inase treatment.

the mTORC1 signaling pathway (**Figure 3.4c**) in all 3 cell lines. In the context of cyst(e)inase treatment, GCN2 signaling appeared more important than signaling through AMP kinase (AMPK), another known inhibitor of mTORC1, because sustained AMPK activation was observed in only Panc1 cells even though mTORC1 was inhibited in all three cell lines (**Figure 3.4d**). Since signaling through mTORC1 is intimately tied to cellular anabolism, the inhibition of this pathway provides a mechanistic link for the growth arrest observed with cyst(e)inase treatment in all three cell lines. However, due to the inhibition being present in all three cell lines, the difference in cyst(e)inase sensitivity between the lines begs a different mechanistic explanation.

3.2.5 BSO does not recapitulate effects of cyst(e)inase

To delineate the growth inhibitory effects of cyst(e)inase through GSH depletion versus nutrient deprivation, we treated these same cells with buthionine sulfoximine (BSO), a long-established inhibitor of GSH synthesis. Even though intracellular GSH was completely depleted by BSO within 24 hours in all 3 cell lines, cell survival was unaffected (**Figure 3.5 a,b**). BSO treatment induced cellular ROS (measured by DCFDA) in a manner that was different than that of cyst(e)inase or CSSC-deficient medium treatment (**Figure 3.5 c**). More importantly, BSO treatment did not increase mROS in any of the three cell lines (**Figure 3.5 d**). Therefore, the growth inhibitory and cell killing effects of cyst(e)inase cannot be entirely explained by GSH depletion.

3.3 Discussion

These data show that cysteine/cystine depletion leads to growth inhibition of pancreatic cancer cells. Cyst(e)inase treatment induced ROS stress and subsequently

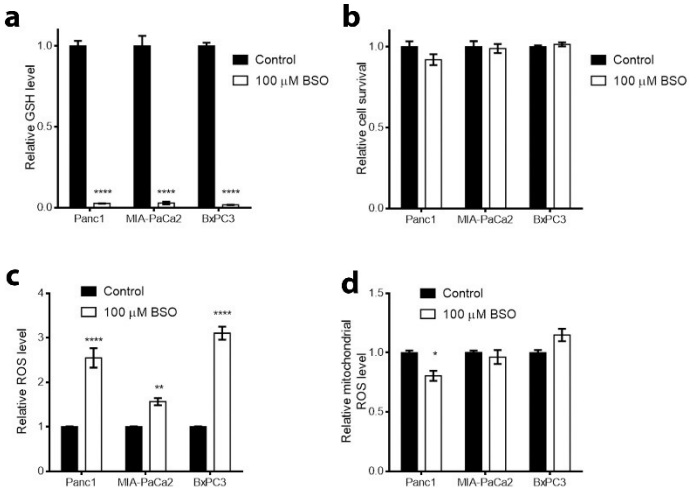

Figure 3.5 Buthionine sulfoximine (BSO) does not recapitulate all the effects of cyst(e)inase in pancreatic cancer cells.

(**a**) Intracellular GSH levels 24 h after treatment (n = 3 technical replicates). (**b**) Relative cell survival 48 h after treatment (n = 3 cultures). (**c**) Cellular ROS levels 24 h after treatment (n = 2-3 independent experiments). (**d**) Mitochondrial ROS levels 24 h after treatment (n = 3-4 independent experiments). All data represent mean ± s.e.m. *$P < 0.05$, **$P < 0.01$, ****$P < 0.0001$; compared to untreated controls; two-way ANOVA with Bonferroni's method for multiple-comparison test.

apoptosis in only one (Panc1) of out the three cell lines. A quite unexpected finding was that GSH depletion was not primarily the mechanism of cyst(e)inase mediated cytotoxicity. Cyst(e)inase caused a complete depletion of GSH in all three cell lines but induced ROS accumulation in only Panc1 cells. Buthionine sulfoximine (BSO), a well-known inhibitor of glutamate cysteine ligase (GCL), also caused a complete depletion of GSH but increased the total cellular ROS in a manner that was different than that induced by cyst(e)inase, which surprisingly had no effect on cell survival in any of the cell lines. More importantly, only cyst(e)inase and not BSO caused an increase in mitochondrial superoxide (mROS) in Panc1 cells implicating mitochondrially derived ROS as the major agent inflicting oxidative stress and mediating sensitivity to cyst(e)inase. Furthermore, a non-proliferative phenotype, as induced by cyst(e)inase in the other two "resistant" cell lines, requires changes in nutrient utilization that prioritizes mitochondrial oxidative phosphorylation over glycolysis[9]. Hence, exploring the differences in mitochondrial metabolism between the cell lines might uncover specific adaptations that promote resistance to cyst(e)inase. We can then utilize that knowledge to rationally design combination treatments sensitize the resistant cells to cyst(e)inase.

Chapter 4: Maintaining mitochondrial fitness allows resistant cells to survive during cyst(e)ine deprivation

4.1 Introduction

Altered metabolism is considered a hallmark of cancer[11]. Almost a century ago, Otto Warburg noticed the ability of tumor cells to rapidly convert glucose into lactate through glycolysis even in the presence of oxygen, now famously known as the Warburg Effect, and hypothesized mitochondrial dysfunction as a central tenet of cellular transformation. However, research in cancer metabolism over the last two decades has uncovered the indispensable nature of the biosynthetic and bioenergetic functions of the mitochondria in supporting cell survival and proliferation, which has deemed Warburg's original hypothesis untenable[12,72]. Moreover, cancer cells are known to rely more on mitochondrial oxidative phosphorylation to maintain survival during nutrient limiting conditions[9,73]. Since the two cyst(e)inase-resistant cell lines are able to switch to a non-proliferative phenotype and maintain survival during L-Cys/CSSC, we took the next logical step of exploring the mitochondrial metabolic network in these cell lines. In this chapter, we show that only the resistant cell lines are able to maintain biosynthetic and bioenergetic functions of the mitochondria during cyst(e)inase treatment, and concurrently inhibiting those functions leads to synergistic inhibition of cell survival.

4.2 Results

4.2.1 Cyst(e)inase causes anaplerosis defect in only Panc1

Within just 3 hours of cyst(e)inase treatment, there was a marked increase in succinate levels in MIA-PaCa2 cells, which returned close to normal levels by 24 hours;

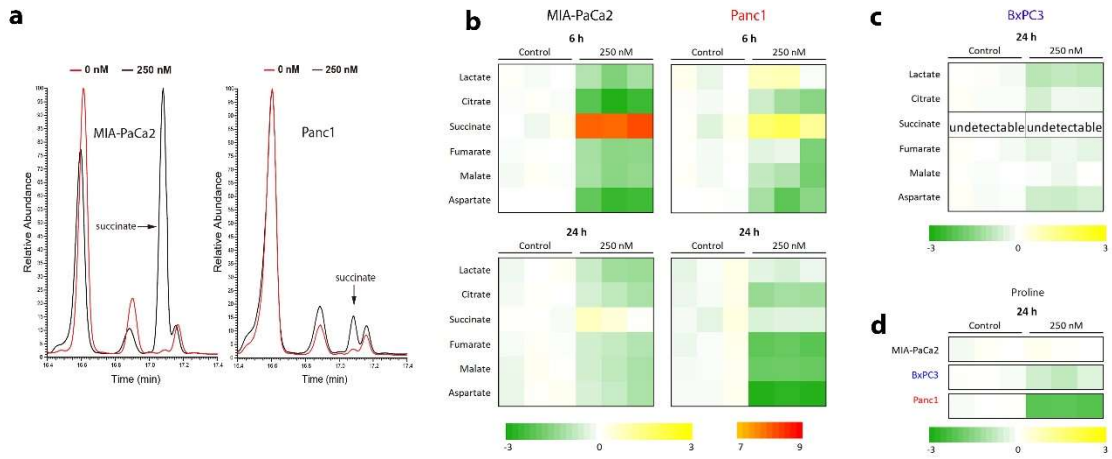

Figure 4.1 Cyst(e)inase causes anaplerotic defect in only Panc1 cells.

(**a**) Intracellular succinate abundance in MIA-PaCa2 and Panc1 cells 3 h after cyst(e)inase treatment. (**b**)TCA cycle intermediates and related metabolite levels 6 h and 24 h after 250 nM cyst(e)inase treatment in MIA-PaCa2 and Panc1 cells (n = 3 cultures). (**c,d**) TCA cycle intermediates and related metabolite levels in BxPC3 cells (**c**; n = 3 cultures) and proline levels in all 3 cell lines (**d**; n = 3 cultures) 24 h after cyst(e)inase treatment. For **b-d**, color bar shows Log_2 scale.

this increase was comparatively mild in Panc1 (**Figure 4.1 a,b**). Cyst(e)inase treatment in MIA-PaCa2 and Panc1 cells seemingly produces a blockade of the tricarboxylic acid (TCA) cycle at succinate dehydrogenase (SDH, Complex II), which catalyzes the oxidative conversion of succinate to fumarate using the electron acceptor FAD. A complete truncation of the TCA cycle without a mechanism to replenish pools of downstream metabolites cannot support cell proliferation because aspartate, which is derived from oxaloacetate (OAA) and contributes to nucleic acid and protein synthesis, is a limiting nutrient for cell proliferation[25,26] (**Illustration 4.1**). Oxaloacetate in proliferating cells is generally derived via anaplerosis from glutamine[27]. However, cells that are deficient in SDH or cells that overcome glutamine dependence require upregulation of pyruvate carboxylase (PC) to replenish pools of aspartate[29-31] (**Illustration 4.1**). The initial drop in aspartate levels following cyst(e)inase treatment eventually recovered in MIA-PaCa2 cells (to more than 50% of control) whereas it continued to drop in Panc1 cells (to less than 15% of control) (**Figure 4.1 b**). The blockade in SDH (indicated by succinate accumulation) was not seen in BxPC3 cells; concomitantly, they were also able to maintain aspartate levels at more than 50% of control upon cyst(e)inase treatment (data not shown and **Figure 4.1 c**) most likely through glutamine dependent anaplerosis (further elaborated in **Chapter 4.2.2**). Further supporting the fact that Panc1 cells became deficient in glutamine-dependent anaplerosis after cyst(e)inase treatment was that proline, a glutamine derived amino acid, was markedly depleted only in Panc1 cells (**Figure 4.1 d**).

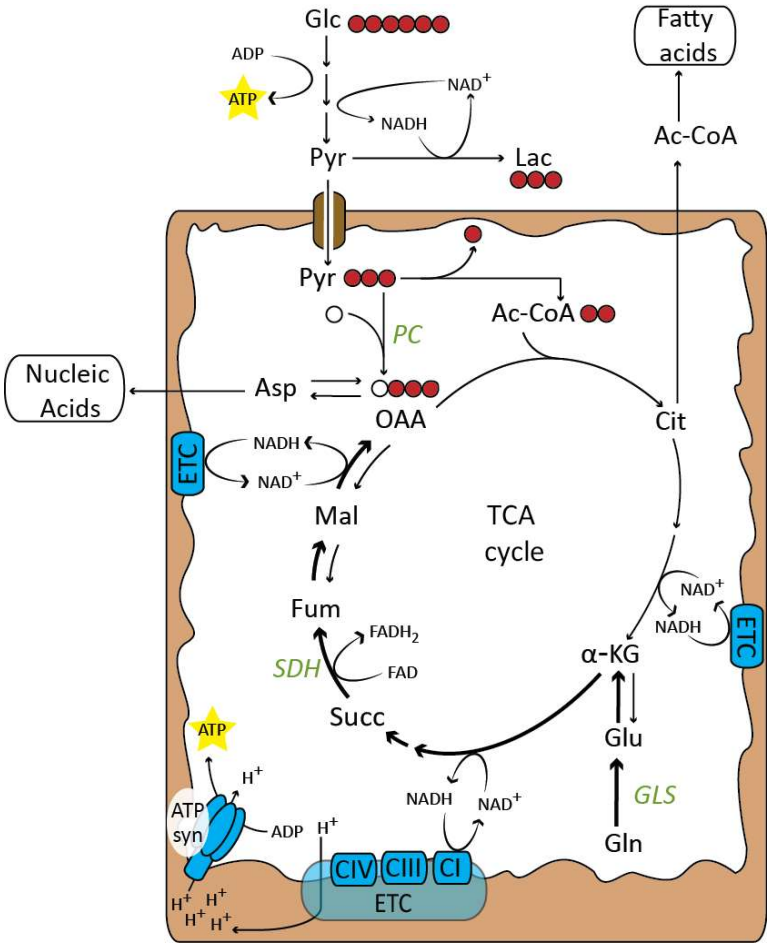

Illustration 4.1 Schematic of nutrient utilization through the TCA cycle.

Predicted induction of pyruvate carboxylase (PC) activity by MIA-PaCa2 cells to replenish pools of oxaloacetate (OAA) and subsequently aspartate (Asp) via [U-^{13}C]-glucose. Abbreviations: Glc, glucose; Pyr, pyruvate; Lac, lactate; Ac-CoA, acetyl-CoA; Cit, citrate; α-KG, α-ketoglutarate; Glu, glutamate; Gln, glutamine; Succ, succinate, Fum, fumarate; Mal, malate; GLS, glutaminase; SDH, succinate dehydrogenase; ETC, electron transport chain; ATP syn, ATP synthase.

4.2.2 Resistant cells maintain anaplerosis during L-Cys/CSSC deprivation

As aforementioned, a truncation of the TCA cycle without a mechanism to replenish downstream metabolites is incompatible with cell survival and proliferation. We therefore compared induction of PC activity between MIA-PaCa2 and Panc1 cells upon cyst(e)inase treatment by culturing these cells in [U-^{13}C]-glucose (glucose labeled in all 6 carbons with ^{13}C). Anaplerosis through PC, which catalyzes the carboxylation of glucose-derived pyruvate to form oxaloacetate, is expected give rise to m+3 mass isotopologue (metabolite labeled with ^{13}C in 3 of its carbons) in the aspartate pool as illustrated in **Illustration 4.1**. On the other hand, oxidation of pyruvate into acetyl-CoA through pyruvate dehydrogenase (PDH) and subsequent entry into the TCA cycle gives rise to m+2 mass isotopologues in downstream metabolites. MIA-PaCa2 cells were able to recover their aspartate levels via anaplerosis through PC as evidenced by an increase in m+3 fraction in aspartate and all the way to fumarate; this compensatory upregulation of PC activity was absent in Panc1 cells (**Figure 4.2 a,b**). The absence of cyt(e)inase-mediated SDH blockade in BxPC3 cells (**Chapter 4.2.1**) obviated the need for PC upregulation in these cells (**Figure 4.2 c**). Glutamine-dependent anaplerosis of the TCA cycle appeared unperturbed and enough to maintain aspartate levels in BxPC3 and consequently promote cell survival during L-Cys/CSSC deprivation, which was supported by two observations. First, the unlabeled (m+0) fraction of aspartate and fumarate in [U-^{13}C]-glucose cultured cells, normally a surrogate measure of glutamine-dependent anaplerosis, was unchanged with cyst(e)inase treatment (**Figure 4.2 c**). Second, combining cyst(e)inase with CB-839, a glutaminase (GLS) inhibitor, produced a synergistic inhibition of cell survival (**Figure 4.2 d**) in BxPC3 cells. Furthermore, the cyst(e)inase-resistant cells (MIA-PaCa2 and BxPC3) exhibited a higher basal glutamine utilization in the TCA cycle as assessed by a

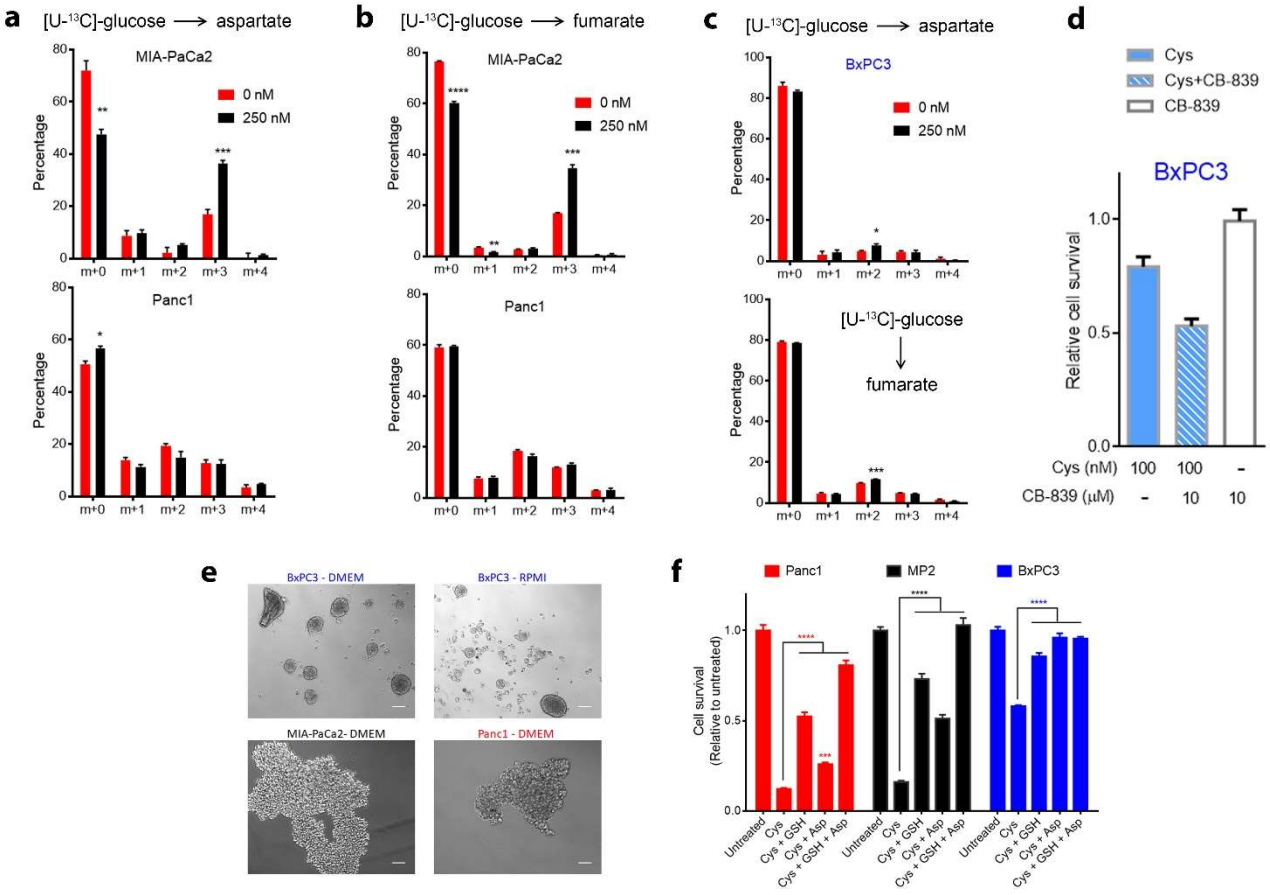

Figure 4.2 Anaplerosis through glucose and glutamine in resistant cells.

(**a,b**) Mass isotopologue analysis of aspartate (**a**) and fumarate (**b**) in MIA-PaCa2 (top) and Panc1 cells (bottom) cultured in [U-^{13}C]-glucose and treated with cyst(e)inase for 6 h (n = 3 cultures). (**c**) Mass isotopologue analysis of aspartate (top) and fumarate (bottom) in BxPC3 cells cultured in [U-^{13}C]-glucose and treated with cyst(e)inase for 6 h (n = 3 cultures). (**d**) Cell survival of BxPC3 cells treated with combination of cyst(e)inase (Cys) and CB-839 for 48 h. Values are relative to untreated control, which is not shown (n = 3 cultures for each condition). (**e**) Spheroid formation capacity assessed 3 days after plating. BxPC3 cells were cultured in both RPMI and DMEM. Scale bars, 100 μm. (**f**) Relative cell survival 48 h after treatment with either 200 nM Cys alone or in combination (single or double) with 0.5 mM GSH ethyl ester (GSH) and 5 mM methyl aspartate (Asp) (n = 3 cultures). All data represent mean ± s.e.m. *P < 0.05, **P < 0.01, ***P < 0.001, ****P < 0.0001; compared to untreated controls (**a**-**c**) or to Cys treatment (**f**); two-sided Student's t-test (**a**-**c**) or two-way ANOVA with Bonferroni's method for multiple-comparison test (**f**).

higher m+0 fraction in fumarate and aspartate (**Figure 4.2 1 a-c**). In addition, BxPC3 cells also appeared to have an increased capacity to rewire glutamine metabolism as evidenced by the fact that only these cells easily acquired anchorage independence and formed spheroids, a process that requires reductive carboxylation of glutamine-derived α-ketoglutarate for maintenance of mitochondrial redox homeostasis[74] (**Figure 4.2 e**). Supplementing cyst(e)inase with cell-permeable forms of GSH and aspartate as single agents rescued cell survival partially in all 3 cell lines but the two in combination augmented cell survival to untreated levels in MIA-PaCa2 and BxPC3 and near-untreated levels in Panc1 (**Figure 4.2 f**), bolstering our argument that GSH depletion is not the only mechanism through which cyst(e)inase mediates inhibition of cell survival. The mechanism of rescue with GSH ethyl ester in MIA-PaCa2 and BxPC3, in which cyst(e)inase did not induce oxidative stress, could be through normalization of redox sensitive protein signaling[75] or cleavage of this GSH at the cell surface by gamma-glutamyl transpeptidase/transferase followed by passive diffusion of Cys-Gly-ethyl ester dipeptide inside the cell and subsequent hydrolysis to produce intracellular L-Cys[76,77].

4.2.3 Synergy through inhibition of mitochondrial metabolism

To provide proof-of-principle that maintaining mitochondrial fitness is integral for acquiring resistance to cyst(e)inase, we attempted to concurrently inhibit mitochondrial metabolism at different nodes. Corroborating our previous finding that BxPC3 cells rely on glutamine metabolism to support cell survival during cyst(e)inase treatment, BxPC3 were the most sensitive out of the three lines to concurrent glutaminase inhibition by CB-839 (**Figure 4.3 a**). Since, MIA-PaCa2 cells exhibited upregulation of PC activity with

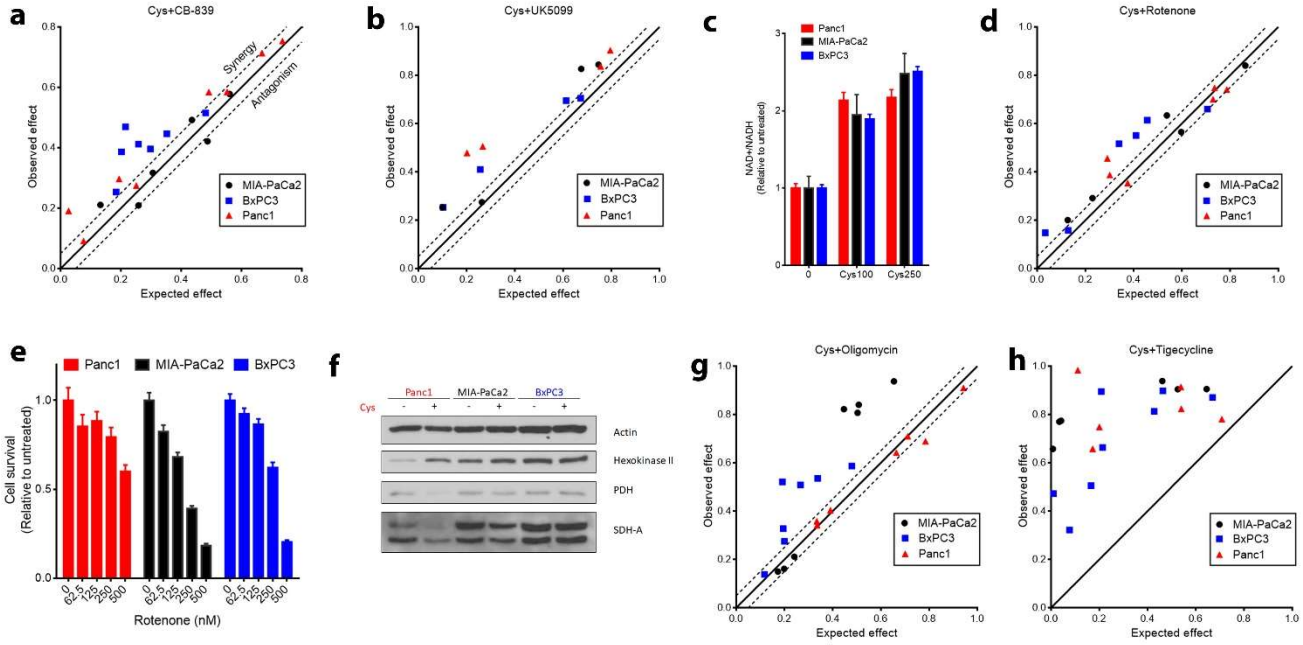

Figure 4.3 Inhibition of mitochondrial metabolism synergizes with cyst(e)inase.

(**a,b**) Isobologram of the effect of the combination of cyst(e)inase (Cys) and CB-839 (**a**), and Cys and UK5099 (**b**) (data from 2-4 independent experiments). (**c**) Intracellular ratio of NAD+/NADH 24 h after cyst(e)inase treatment (n = 3 cultures). (**d**) Isobologram of the effect of the combination of Cys and rotenone (data from 3 independent experiments). (**e**) Relative cell survival 48 h after rotenone treatment (n = 3 cultures for each dose). (**f**) Comparison of metabolic enzymes. "+" represents 250 nM cyst(e)inase treatment. (**g,h**) Isobologram of the effect of the combination of Cys and oligomycin (**g**), and Cys and tigecycline (**h**) (data from 3-4 independent experiments). For **c** and **e**, data represent mean ± s.e.m.

cyst(e)inase treatment, we concurrently blocked pyruvate transport into the mitochondrial matrix with the compound UK5099[28]. Inhibiting mitochondrial pyruvate transport with UK5099 had a mild synergistic effect in all 3 cell lines (**Figure 4.3 b**), not only due to abrogation of PC activity but possibly also due to depletion of citrate, which is important for fatty acid synthesis (**Illustration 4.1**). We established in **Chapter 4.2.2** that maintaining aspartate synthesis is an important factor for maintaining survival during L-Cys/CSSC deprivation. A major requirement for the biosynthesis of aspartate is the proper functioning of the electron transport chain and maintenance of the NAD+/NADH ratio[25,26]. The depletion of aspartate seen with cyst(e)inase treatment only in Panc1 cells was not due to a perturbation of this ratio, and combining cyst(e)inase with rotenone (inhibitor of Complex I, which recycles NADH into NAD+) induced only a mild synergistic effect (**Figure 4.3 c,d**). It was notable however that MIA-PaCa2 and BxPC3 cells were more sensitive to rotenone treatment indicating that they have an increased basal reliance on the electron transport chain (**Figure 4.3 e**). Further supporting the idea that Panc1 cells cannot maintain mitochondrial metabolism during L-Cys/CSSC deprivation was that cyst(e)inase induced an increase in the glycolytic enzyme hexokinase with concomitant decrease in the mitochondrial enzymes pyruvate dehydrogenase (PDH) and succinate dehydrogenase-A (SDH-A) (**Figure 4.3 f**). There was no stark difference between the three lines in basal reliance on ATP synthase as probed by its inhibitor oligomycin (data not shown), but interestingly, MIA-PaCa2 and BxPC3 could be sensitized to cyst(e)inase through concurrent oligomycin treatment (**Figure 4.3 g**) corroborating the notion that a quiescent, non-proliferative phenotype requires oxidative phosphorylation[9]. The most compelling evidence for our mitochondrial fitness hypothesis is provided by the fact that tigecycline, an approved antibiotic that inhibits mitochondrial protein translation, produces a strong synergistic effect with cyst(e)inase in all three cell lines (**Figure 4.3 h**).

4.3 Discussion

We have discovered here that resistance to cyst(e)inase is predicated on the ability to maintain mitochondrial function despite L-Cys/CSSC depletion. Specifically, resistant cells are able to sustain anaplerosis of the TCA cycle for aspartate synthesis and maintain ETC function for cellular bioenergetics. In MIA-PaCa2 cells, cyst(e)inase induced a block in SDH of the TCA cycle, which necessitated compensatory upregulation of PC activity for anaplerosis. The canonical route of anaplerosis through glutamine appeared unperturbed in BxPC3 cells. In the sensitive Panc1 cells however, cyst(e)inase induced a defect in glutamine-dependent anaplerosis that was not compensated by PC upregulation. Consequently, the aspartate levels in Panc1 cells fell to very low levels, which is consistent with the observation that cells that cannot utilize alternate fuel sources for anaplerosis during glutamine starvation are susceptible to ROS accumulation[28]. In Panc1 cells, cyst(e)inase reduced expression of SDH-A, which could explain the observed anaplerotic defect, as well as PDH. Interestingly, both of these mitochondrial flavoproteins, PDH and SDH-A, are known to be sites of ROS production[78], yet their important bioenergetic role is highlighted by the fact that their loss can precipitate a progressive neurodegenerative disease called Leigh Syndrome characterized by dysfunctional mitochondrial energy production[79,80]. Concurrently inhibiting mitochondrial metabolism at different nodes produced synergistic inhibition of cell survival with cyst(e)inase treatment. These data suggest that perturbing the biosynthetic and bioenergetic functions of the mitochondria could be a viable approach to obtain synergy with cyst(e)inase, a strategy that we will build upon in **Chapter 5**.

Chapter 5: Auranofin synergizes with cyst(e)inase by increasing mitochondrial ROS and inhibiting mitophagy

5.1 Introduction

In **Chapter 4**, we explored the differences in mitochondrial metabolism between Panc1 and the other two cyst(e)inase-resistant cells and discovered that the biosynthetic and bioenergetic functions of the mitochondria constitute synthetically lethal targets with cyst(e)inase. However, a caveat of this approach is that since mitochondrial functions are integral to the survival of non-cancerous cells as well, the therapeutic window that can be achieved through this strategy is likely very narrow. Indeed, strong inhibitors of the some parts of the mitochondrial respiratory complex (i.e., cyanide) are well-established lethal agents. Even tigecycline, which exhibited a high degree of synergy with cyst(e)inase in our studies, despite being an FDA-approved antibiotic, is used as a last-resort drug due to its unexplained higher mortality risk[81]. Alternately, complex I of the mitochondrial electron transport chain can be inhibited by metformin[82], a biguanide anti-diabetic drug with an excellent safety profile; however, a stronger complex I inhibitor in rotenone produced only a mild synergistic effect with cyst(e)inase (**Figure 4.3 d**) indicating that complex I is likely not a very effective synthetic lethal target.

Another approach at obtaining synergy with cyst(e)inase is concurrently inhibiting antioxidant pathways since maintaining mitochondrial function comes with the liability of detoxifying ROS, majority of which is produced by the ETC[42]. In this chapter, we demonstrate that inhibiting alternate antioxidant pathways is an excellent approach of achieving synergy with cyst(e)inase in pancreatic cancer cells.

5.2 Results

5.2.1 The thioredoxin system: a prime target for synergy

Comparison of antioxidant pathways in the three cell lines indicated that basal levels of glutamate-cysteine ligase (GCL-C, enzyme involved in glutathione synthesis), cystine/glutamate antiporter (xCT) and thioredoxin1 were highest in BxPC3 (**Figure 5.1 a**). Levels of the transcription factor nuclear factor (erythroid-derived 2)-like 2 (Nrf2), a master regulator of cellular antioxidant response[42] were also analyzed. Cyst(e)inase treatment caused induction of Nrf2 that was immediate and sustained in Panc1 but minimal in BxPC3 (**Figure 5.1 b**); hence Nrf2's antioxidant response did not correlate with resistance to cyst(e)inase. Cystine deprivation is known to induce xCT in these particular cell lines[83], which was recapitulated by cyst(e)inase treatment and as a result, the stark difference in xCT between the untreated cells was diminished (**Figure 5.1 c**). Such induction was not seen in GCL-C and thioredoxin1 (**Figure 5.1 c**). Concurrent inhibition of xCT with sulfasalazine produced synergy with cyst(e)inase in all three cells, but not as much as with inhibition of GCL using BSO (**Figure 5.1 d,e**). The lower synergy observed with sulfasalazine is probably due to the induction of xCT, which likely plays a protective role to some degree by facilitating increased cystine import. The synergy observed with BSO has a caveat as BSO is not yet approved for use in the clinic. We therefore turned to thioredoxin 1 whose expression pattern was especially striking because it was positively correlated with resistance to cyst(e)inase. Thioredoxins are antioxidant proteins that scavenge ROS by cycling between oxidized and reduced forms with the help of thioredoxin reductases. Mammalian cells have two major isoforms – a cytosolic thioredoxin 1 and a mitochondrial thioredoxin 2 that pair up with thioredoxin reductases 1 and 2 (TXNRD1 and TXNRD2), respectively. Auranofin inhibits both isoforms of thioredoxin reductase[84]

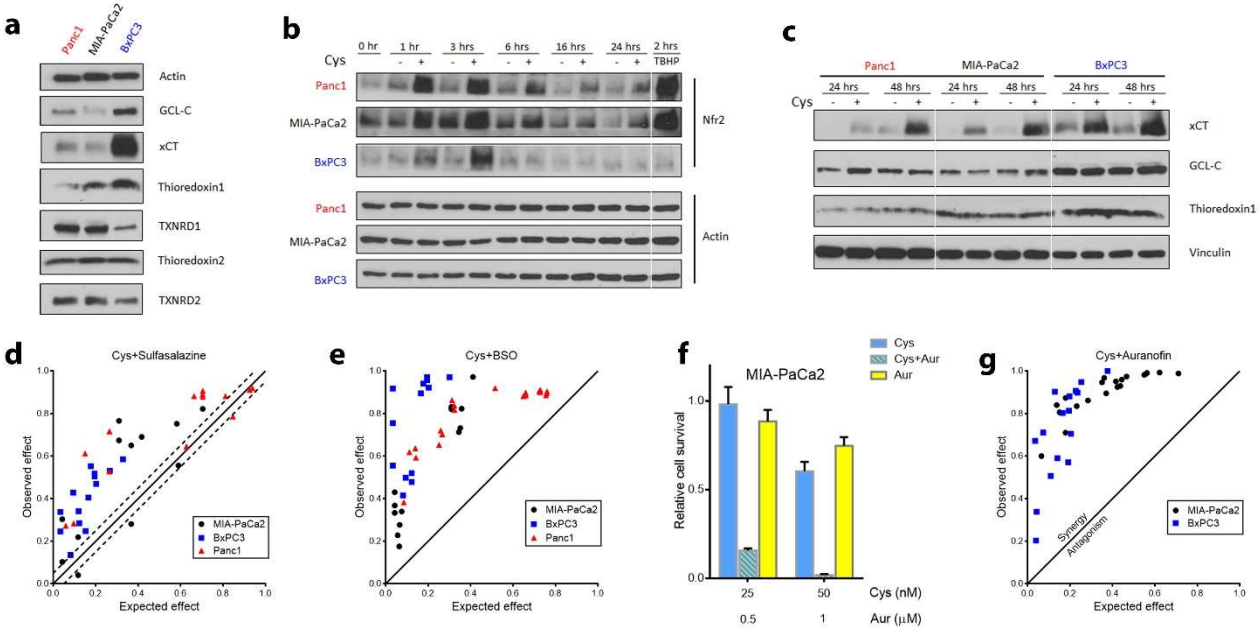

Figure 5.1 Inhibition of alternate antioxidant pathways synergizes with cyst(e)inase.

(**a**) Comparison of proteins related to antioxidant function in the 3 cell lines. Abbreviations: GCL-C, glutamate-cysteine ligase catalytic subunit; xCT, cystine/glutamate antiporter; TXNRD1 and TXNRD2, thioredoxin reductase 1 and 2 respectively. (**b, c**) Expression of antioxidant proteins following cyst(e)inase treatment. TBHP treatment (200 μM, 2 h) is included as a positive control for ROS accumulation (**c**). (**d,e**) Isobologram of the effect of the combination of cyst(e)inase (Cys) and sulfasalazine (**d**), and Cys and BSO (**e**) (data from more than 3 independent experiments). (**f**) Cell survival of MIA-PaCa2 cells treated with combination of Cys and auranofin (Aur) for 48 h. Values are relative to untreated control, which is not shown (n = 3 cultures for each condition). (**g**) Isobologram of the effect of the combination of Cys and auranofin in MIA-PaCa2 and BxPC3 cells (data from more than 3 independent experiments). For **b** and **c**, "+" represents 250 nM cyst(e)inase treatment except for **c**, where "+" for Panc1-48 hrs represents 100 nM treatment. For **f**, data represent mean ± s.e.m.

and is also an approved drug (Ridaura®) for the treatment of rheumatoid arthritis. As expected, auranofin treatment sensitized both of the resistant cell lines to cyst(e)inase (**Figure 5.1 f,g**).

5.2.2 Auranofin and cyst(e)inase synergize through mitochondrial ROS

As cytotoxicity induced by L-Cys/CSSC deprivation in Panc1 cells was specifically correlated with mitochondrial ROS (**Chapter 3**), we assessed mROS accumulation and oxidative stress signaling in the two resistant cell lines when treated with combination of cyst(e)inase and auranofin. The synergistic decrease in cell survival induced by combination treatment was paralleled with synergistic increases in mROS and cell death, which was rescued by supplementation with cell-permeable GSH (**Figure 5.2 a**). CSSC-deficient medium combined with auranofin recapitulated the synergistic increase in cell death (**Figure 5.2 b**). Parameters of oxidative stress and DNA damage (activation of ATM and H2AX, and upregulation of c-Jun via activation of JNK) as well as markers of apoptosis (cleavage of ATM, PARP, and caspases 3 and 7) were increased by combination treatment and rescued by GSH supplementation (**Figure 5.2 c**). Moreover, growth-promoting cell cycle checkpoint proteins (phosphorylated retinoblastoma, cdk1, cdc25C) were decreased and the inhibitory cell cycle protein p27 was increased by the combination of cyst(e)inase and auranofin (**Figure 5.2 d**). Mitochondrial ROS induced by the combination was capable of reaching the nucleus to cause the observed genotoxic effects (**Figure 5.3 a,b**).

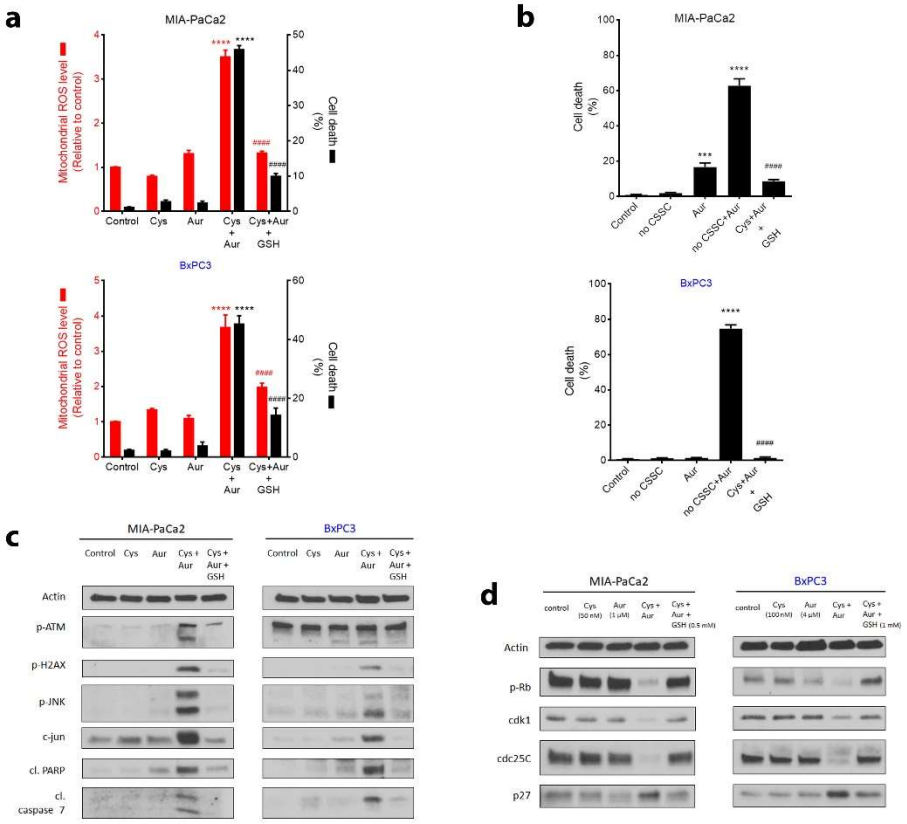

Figure 5.2 Cyst(e)inase and auranofin combination treatment induces mROS and apoptosis in cyst(e)inase-resistant cells.

(**a**) Relative mitochondrial ROS (mROS) levels (red) and cell death (black) in MIA-PaCa2 (top) and BxPC3 (bottom) cells 24 h after indicated treatments. MIA-PaCa2: 50 nM Cys, 0.5 μM (mROS) or 2 μM (cell death) Aur, BxPC3: 100 nM Cys, 2 μM (mROS) or 4 μM (cell death) Aur; 0.5 mM GSH ethyl ester (GSH) for both cell lines (for mROS, $n = 5$ independent experiments; for cell death, $n = 3$ independent experiments). (**b**) Cell death in MIA-PaCa2 (top) and BxPC3 (bottom) cells 24 h after treatment with cystine (CSSC) deficient media, its combination with Aur (BxPC3: 4 μM, MIA-PaCa2: 2 μM) and the combination plus GSH (BxPC3: 0.5 mM, MIA-PaCa2: 1 mM) ($n = 3$ independent experiments). (**c**) Oxidative stress markers and apoptosis signaling in MIA-PaCa2 and BxPC3 cells treated with similar concentrations as in (**a**). (**d**) Regulatory cell cycle proteins 24 h after the indicated combinatorial treatments in MIA-PaCa2 and BxPC3 cells. All data represent mean ± s.e.m. For **a** and **b,** ####P or ****$P < 0.0001$; compared to untreated controls (*, comparison done for Cys or no CSSC, Aur and Cys+Aur) or to Cys+Aur (#, comparison done for only Cys+Aur+GSH); one-way ANOVA with Bonferroni's method for multiple-comparison test.

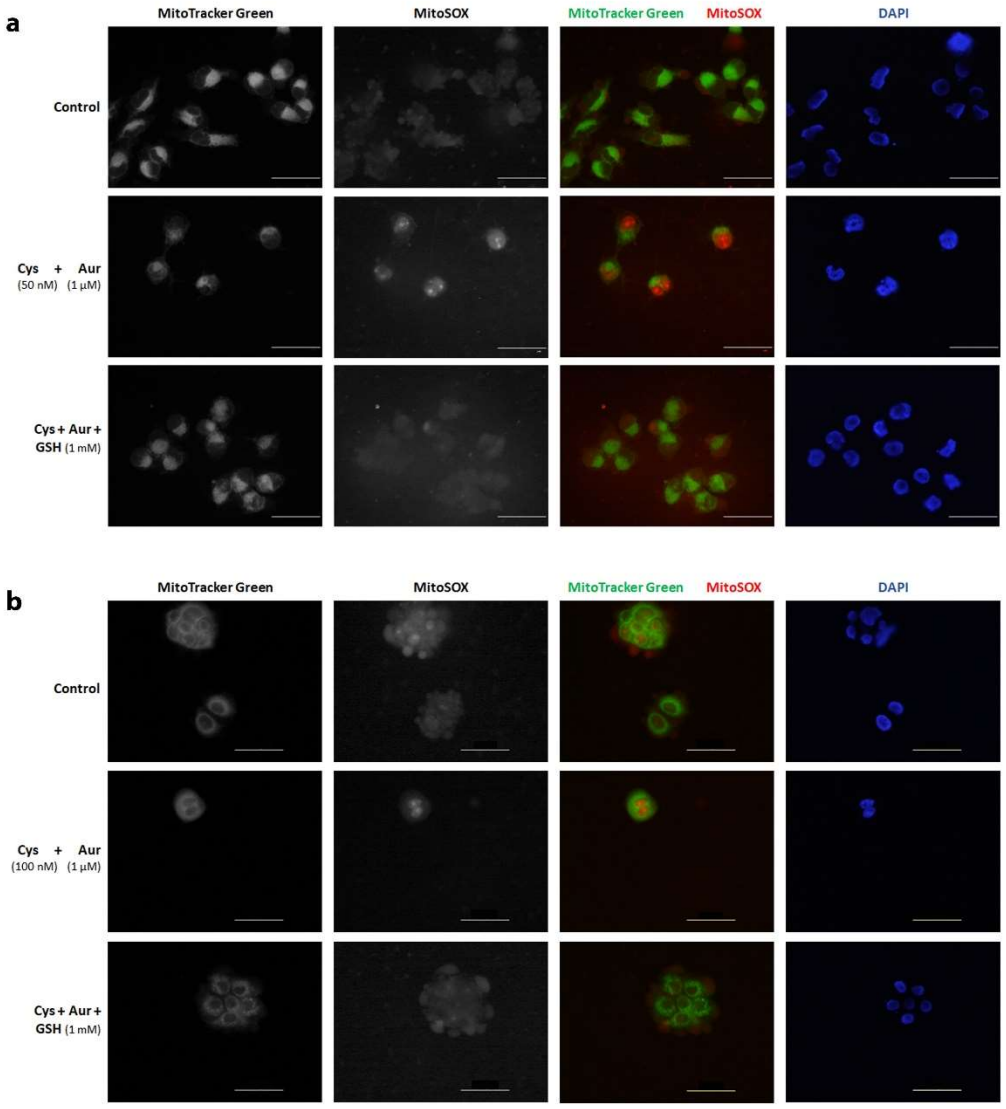

Figure 5.3 Mitochondrial ROS induced by combination treatment of cyt(e)inase and auranofin reaches the nucleus.

(**a,b**) Representative images show mitochondrial ROS production in MIA-PaCa2 (**a**, 12 h treatment) and BxPC3 (**b**, 24 h treatment) cells labeled with MitoTracker Green and MitoSOX after indicated combinatorial treatments. Scale bars, 100 μm.

5.2.3 Inhibition of mitophagy and defective mitochondrial clearance

We also investigated the effect of combination treatment on autophagy given its role in mitochondrial quality control and found an inhibition of autophagic flux as indicated by accumulation of both forms of LC3 protein as well as p62 (**Figure 5.4 a**). MIA-PaCa2 cells transfected with mCherry-GFP-LC3 construct demonstrated that this autophagic defect is due to failure of autolysosome formation evidenced by an increase in colocalization of red and green fluorescence (yellow puncta), which was also seen in cells treated with Bafilomycin A1, an inhibitor of autophagosome and lysosome fusion[85] (**Figure 5.4 b,c**). This block in autophagy caused an accumulation of defective mitochondria that cannot maintain membrane potential (**Figure 5.4 d-g**), which are more prone to producing ROS[69]. Since GSH supplementation rescued this inhibition of mitophagy (**Figure 5.4 a-g**), ROS stress appeared to be the inciting event which supports the idea that the cyst(e)inase and auranofin combination is likely causing a vicious cycle of ROS stress and accumulation of defective mitochondria. In addition to oxidative damage, the loss of mitochondrial fitness abrogates the ability of cyst(e)inase-resistant cells to survive under L-Cys/CSSC deprivation.

5.2.4 Thioredoxin reductase: the main target for synergy

We next attempted to recapitulate these results with genetic inhibition of thioredoxin reductase. Surprisingly, knocking down thioredoxin reductases 1 and 2 individually as well as concurrently had little or no combinatorial effect together with cyst(e)inase treatment (**Figure 5.5 a-c**). However, further analyses showed that a concentration of auranofin that reduces total thioredoxin reductase activity to the same level as that achieved by the double knockdown (~50% of control) also did not produce a

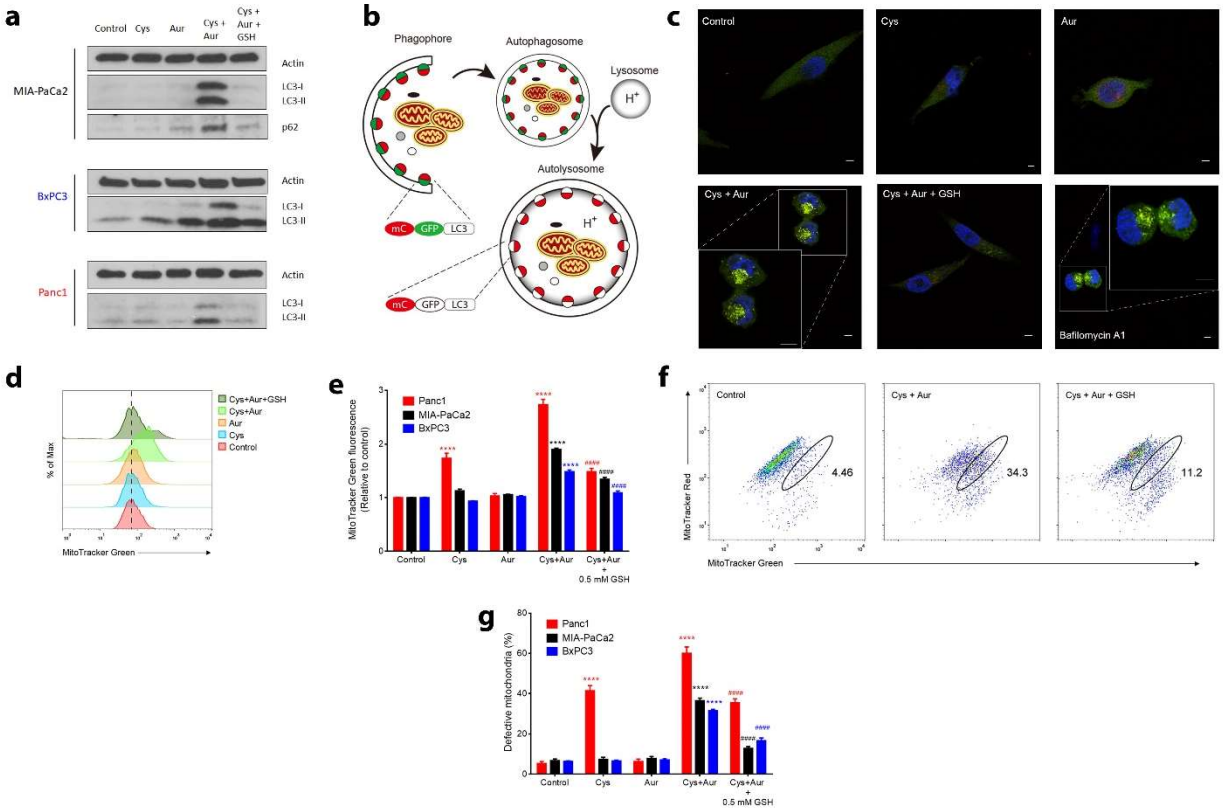

Figure 5.4 Combination treatment of cyt(e)inase and auranofin inhibits mitophagy and causes accumulation of defective mitochondria.

(**a**) Autophagy signaling 24 h after the indicated combinatorial treatments. (**b**) The doubly-tagged mCherry-GFP-LC3 protein emits both red and green fluorescence (yellow when merged) from autophagosomes but only red fluorescence after fusion with lysosome due to quenching of GFP in the acidic environment of the autolysosome (**c**) Confocal microscopy images of mCherry-GFP-LC3-transfected MIA-PaCa2 cells 6 h after indicated treatments (Cys: 250nM, Aur: 0.5 μM, GSH: 2 mM, Bafilomycin A1: 10 nM; data from a representative experiment). Scale bars, 5 μm. (**d**) Mitochondrial mass was analyzed by labeling MIA-PaCa2 cells with MitoTracker Green. (**e**) Quantification of MitoTracker Green fluorescence after indicated combinatorial treatments for 24 h (n = 3-4 independent experiments). (**f**) Mitochondrial membrane potential ($\Delta\psi_m$) was analyzed by labeling MIA-PaCa2 cells with MitoTracker Green and MitoTracker Red. Gated population represents cells containing mitochondria with decreased membrane potential. (**g**) Quantification of cells with defective mitochondrial membrane potential after indicated combinatorial treatments for 24 h (n = 4 independent experiments). All data represent mean ± s.e.m. ####P or ****$P < 0.0001$; compared to untreated controls (*, comparison done for Cys or no CSSC, Aur and Cys+Aur) or to Cys+Aur (#, comparison done for only Cys+Aur+GSH); two-way ANOVA with Bonferroni's method for multiple-comparison test.

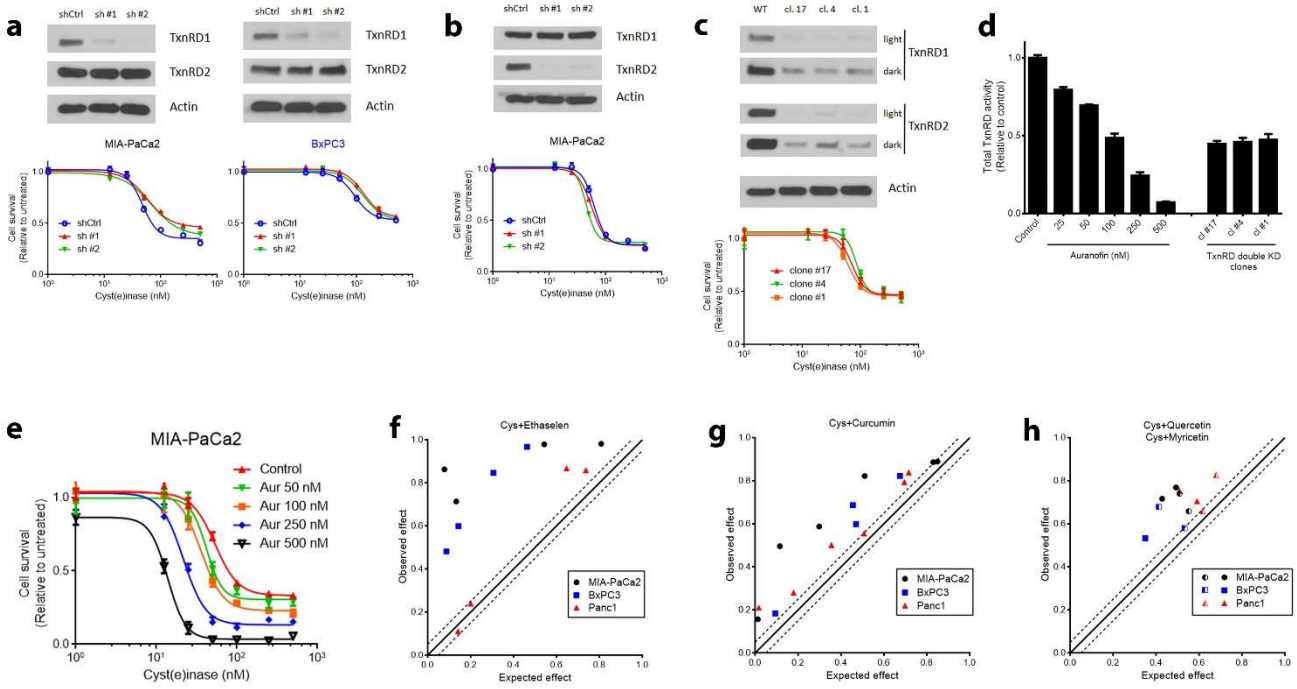

Figure 5.5 Thioredoxin reductase is the synergistic target for auranofin but a near-complete inhibition is required.

(**a,b**) Relative cell survival 48 h after cyst(e)inase treatment in cells harboring shRNA-mediated knockdown of thioredoxin reductase 1 (**a**) and thioredoxin reductase 2 (**b**) (*n* = 3 cultures for each dose). (**c**) Relative cell survival 48 h after cyst(e)inase treatment in clones (cl.) of MIA-PaCa2 cells harboring shRNA-mediated double knockdown of TXNRD1 and TXNRD2 (*n* = 3 cultures for each dose). (**d**) Total thioredoxin reductase (TxnRD) activity in MIA-PaCa2 cells treated with auranofin for 24 h and in the double knockdown clones from (**c**) (*n* = 3 technical replicates for auranofin treated samples and *n* = 3-4 cultures per clone from two independent experiments). (**e**) Relative cell survival 48 h after cyst(e)inase treatment in MIA-PaCa2 cells treated concurrently with increasing concentrations of auranofin (*n* = 3 cultures for each dose). (**f-h**) Isobologram of the effect of the combination of cyst(e)inase (Cys) and ethaselen (**f**), Cys and curcumin (**g**), Cys and quercetin (**h**, half-filled symbols), and Cys and myricetin (**h**, solid symbols) (data from 2-3 independent experiments).All data represent mean ± s.e.m.

significant combinatorial effect with cyst(e)inase (**Figure 5.5 d,e**). These data suggest a considerable redundancy in the thioredoxin antioxidant system. Additional evidence validating thioredoxin reductase as the major mechanistic target producing synergy in cyst(e)inase and auranofin combination was provided by the fact that synthetic (ethaselen[86]) as well as natural compound inhibitors (curcumin, myricetin, quercetin[87,88]) of thioredoxin reductase produced a synergistic inhibition of cell survival when combined with cyst(e)inase (**Figure 5.5 f-h**).

5.3 Discussion

We demonstrated in **Chapter 4** that the cyst(e)inase-resistant cells were able to survive during L-Cys/CSSC deprivation by maintaining mitochondrial function, inhibiting which produced a synergistic effect with cyst(e)inase. Since the electron transport chain of the mitochondria is a major producer of ROS, we hypothesized that concurrently inhibiting alternate antioxidant pathways might also lead to synergy. As expected, auranofin as well as other inhibitors of antioxidant pathways synergized with cyst(e)inase in our studies. However, dual of inhibition of the GSH (using BSO) and the thioredoxin (using auranofin) antioxidant system to attain synergistic cancer cell killing is not a novel concept[89]. The novelty in our combinatorial approach lies in the mechanistic details.

As described in **Chapter 3**, depletion of GSH is not the only mechanism through which cyst(e)inase mediates cell growth inhibition/apoptosis as BSO was able to recapitulate the former but not the latter. One important consequence of cyst(e)inase and auranofin combination is that in addition to causing an increase in mitochondrial ROS, it also induces a block in autophagic flux. Since one of the major functions of autophagy is to recycle defective organelles (i.e., mitophagy), this block in autophagy led to

accumulation of defective mitochondria, which has two cytotoxic effects that are not entirely mutually exclusive. First, the accumulation of mitochondria with defective membrane potential promotes accumulation of more mROS[69]. Second, the perturbation of mitochondrial metabolism abrogates the ability of cyst(e)inase-resistant cells to maintain the biosynthetic and bioenergetic functions of the mitochondria that promote survival during L-Cys/CSSC depletion. Since detoxifying the accumulated mROS via GSH supplementation was able to reverse the block in mitophagy, the inciting event that precipitates the block appears to be mROS stress. These observations support a model where the combination treatment causes a vicious cycle of mROS production and accumulation of defective mitochondria.

Pancreatic cancers are known to have increased autophagic flux which helps them not only to maintain oxidative metabolism but also to control ROS levels, which makes autophagy inhibition a viable therapeutic target[33,90]. Since our combinatorial approach targets antioxidant mechanisms (GSH and thioredoxin) as well as blocks autophagy, which further exacerbates ROS accumulation and abrogates the resistance to cyst(e)inase imparted by a functional oxidative metabolism, this strategy is likely to prove very effective *in vivo*. In comparison, the combination of BSO and auranofin, even though extremely synergistic *in vitro*, might not be a very effective pharmacological approach at achieving dual inhibition of these antioxidant systems *in vivo* as this combination did not have any significant effects on the growth of lung cancer xenografts[91].

Chapter 6: Cyst(e)inase and auranofin synergizes *in vivo*

6.1 Introduction

To further assess the potential clinical relevance of these findings, we performed studies using xenograft models in mice. Intraperitoneally administered cyst(e)inase has already been shown to be a non-toxic yet effective therapeutic agent in multiple preclinical cancer models[58]. Herein, we show that the *in vivo* sensitivity to cyst(e)inase was similar to what was observed *in vitro*, with Panc1 being the most sensitive and BxPC3 being completely resistant. Further recapitulating our *in vitro* findings, adding auranofin to the treatment regimen sensitized the xenografts of resistant cell lines to cyst(e)inase without any signs of systemic toxicity. We conclude this chapter by presenting a model for the mechanism of action of cyst(e)inase as monotherapy as well as in combination with auranofin, and by presenting preliminary findings from *in vitro* triple-combination experiments that warrant further preclinical exploration.

6.2 Results

6.2.1 Sensitivity profile of cyst(e)inase recapitulated

Biweekly intraperitoneal cyst(e)inase treatment (100 mg/kg) of male nude mice harboring pancreatic cancer xenografts mirrored the in vitro sensitivity profile: Panc1 exhibited the most growth inhibition while BxPC3 xenografts were completely resistant (**Figure 6.1 a-c**). As we previously reported[58], cyst(e)inase treated mice did not show any overt signs of toxicity as their body weight stayed constant for the duration of the treatment (**Figure 6.1 b**).

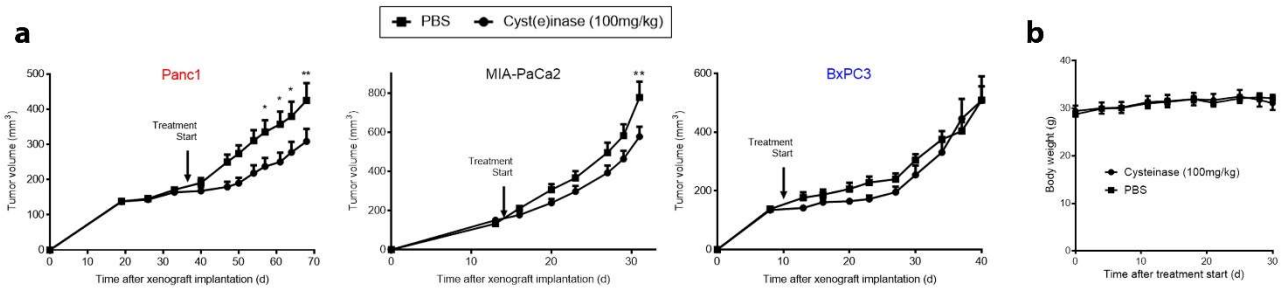

Figure 6.1 Sensitivity to cyst(e)inase is recapitulated in pancreatic cancer xenografts.

(**a**) Growth of xenografted pancreatic tumors in male nude mice treated with cyst(e)inase (n = 8, 7 and 8 mice for Panc1, MIA-PaCa2 and BxPC3 respectively) or PBS control (n = 7, 7 and 9 mice for Panc1, MIA-PaCa2 and BxPC3 respectively). (**b**) Average body weight of mice from BxPC3 xenograft experiment from (**a**). All data represent mean ± s.e.m. *P < 0.05, **P < 0.01, compared to PBS; repeated-measures two-way ANOVA with Bonferroni's method for multiple-comparison test.

6.2.2 Synergy with auranofin recapitulated without toxicity

We next assessed whether the effectiveness of the cyst(e)inase and auranofin combination can be recapitulated *in vivo*. Much to our delight, co-administration of auranofin (3 mg/kg) and cyst(e)inase (100 mg/kg) markedly inhibited the growth of BxPC3 xenografts whereas either agent alone had no significant effect (**Figure 6.2 a**). MIA-PaCa2 cells were more sensitive to combination treatment than BxPC3 cells *in vitro* (**Chapter 5**), so a lower dose of cyst(e)inase was used for the xenograft combination experiment. Isobologram analysis based on the Bliss independence model showed that the combinatorial effects observed in MIA-PaCa2 and BxPC3 xenografts were both synergistic (**Figure 6.2 b,c**). Importantly, the combination did not produce any overt signs of systemic toxicity as body weight and food consumption did not decrease (**Figure 6.2 d**). Moreover, there was no increase in serum ALT (alanine aminotransferase) activity or urea concentration, markers of liver and kidney toxicity, respectively (**Figure 6.2 e**). Immunohistochemical analyses showed that the combination treatment produced focal areas of apoptotic cells (cleaved caspase 3) that exhibited reduced proliferation (Ki67) and reduced mitophagy (LC3 accumulation), which mirrored changes seen in cultured cells treated with the combination. In contrast, tumor regions with cellularity as well as tumors from single-agent treatments did not differ significantly from vehicle treated tumors (**Figure 6.2 f**, data not shown).

6.2.3 A working model and looking ahead

In retrospect, we have demonstrated that cyst(e)inase-mediated L-Cys/CSSC depletion causes mROS accumulation and apoptosis in sensitive pancreatic cancer cells, whereas resistant cells are able to survive this depletion by maintaining mitochondrial

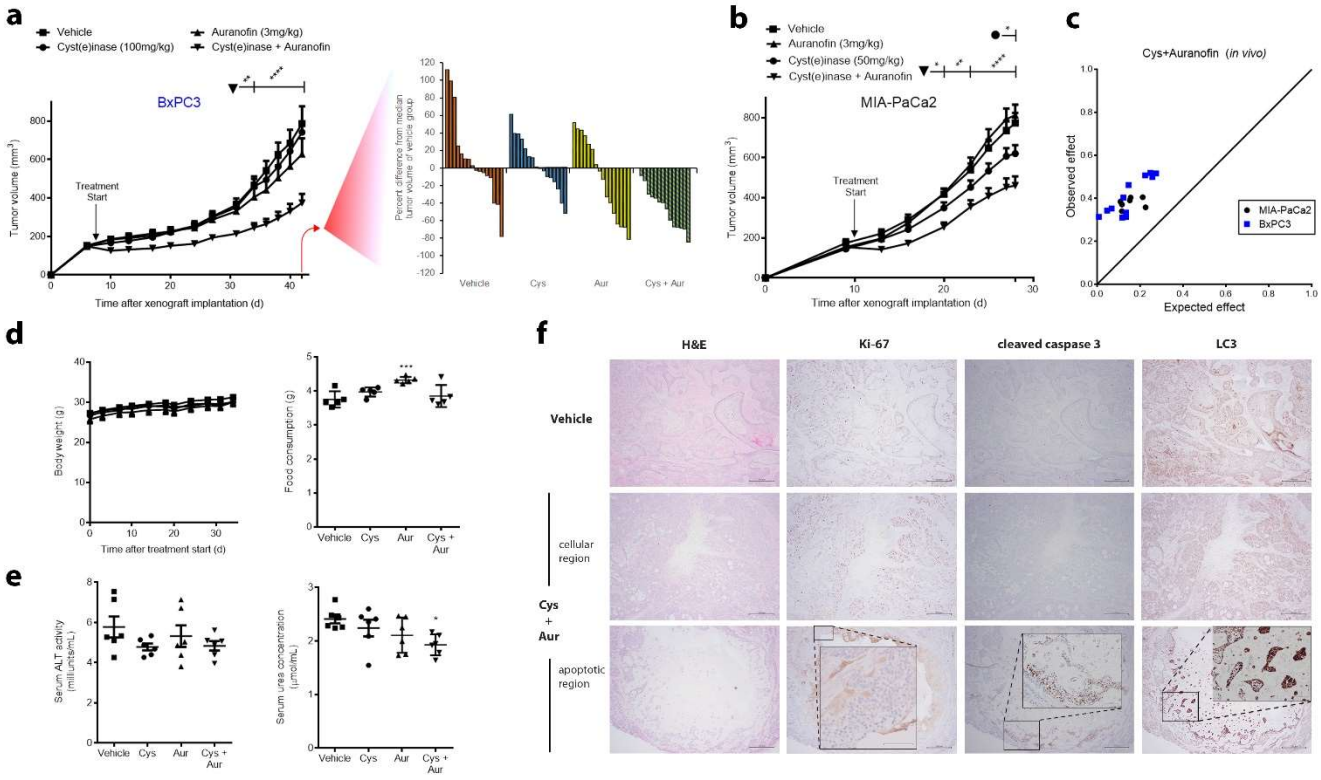

Figure 6.2 Auranofin and cyst(e)inase synergistically inhibit growth of pancreatic cancer xenografts without toxicity.

(**a**) Growth of xenografted BxPC3 pancreatic tumors in male nude mice treated with vehicle control (n = 8 mice), cyst(e)inase (n = 8 mice), auranofin (n = 8 mice), or cyst(e)inase and auranofin in combination (n = 7 mice), and waterfall plots indicating the percent difference from median tumor volume of vehicle treated group at day 42. (**b**) Growth of xenografted MIA-PaCa2 pancreatic tumors in male nude mice treated with vehicle control (n = 8 mice), cyst(e)inase (n = 8 mice), auranofin (n = 9 mice), or cyst(e)inase and auranofin in combination (n = 9 mice). (**c**) Isobologram of the effect of the combination of cyst(e)inase (Cys) and auranofin on BxPC3 and MIA-PaCa2 xenografts. (**d,e**) Average body weight (**d**, left), food consumption (**d**, right), liver toxicity as assessed by serum alanine aminotransferase (ALT) activity (**e**, left), and renal function as assessed by serum urea concentration (**e**, right) in mice from (**a**). (**f**) Representative immunohistochemical staining of xenografts from (**a**). Scale bars, 500 μm (Inset: 100 μm). All data represent mean ± s.e.m. *$P < 0.05$, **$P < 0.01$, ****$P <$ 0.0001; compared to vehicle controls; repeated-measures two-way ANOVA (**a,b**) or two-way ANOVA (**d,e**) with Bonferroni's method for multiple-comparison test.

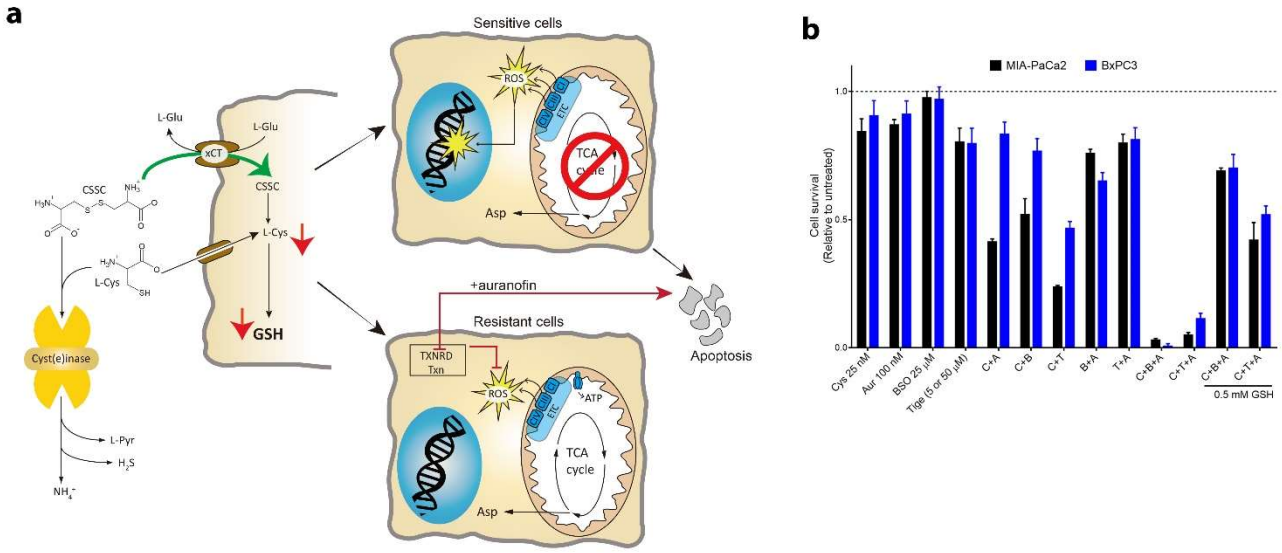

Figure 6.3 A working model and triple combinations with cyst(e)inase for future exploration.

(**a**) Schematic showing basis for sensitivity to cyst(e)inase in pancreatic cancer cells. Cyst(e)inase-mediated depletion of intracellular L-Cys and GSH leads to apoptosis in sensitive cells through mitochondrial dysfunction, which is associated with ROS accumulation and reduced aspartate synthesis for anabolic metabolism. Resistant cells, on the other hand, survive this deprivation by maintaining oxidative metabolism to fuel their biosynthetic and bioenergetic demands, which necessitates detoxification of ROS produced by the electron transport chain (ETC) – a liability that can be clinically targeted by auranofin, a thioredoxin reductase (TXNRD) inhibitor. (**b**) Relative cell survival 48 h after cyst(e)inase treatment after indicated combinatorial treatments (n = 3 cultures for each condition). Values are relative to untreated controls, which is not shown but indicated by dashed line. Abbreviations: Cys or C, cyst(e)inase; Aur or A, auranofin; BSO or B, buthionine sulfoximine, Tige or T, tigecycline. Data represent mean ± s.e.m.

fitness. Consequently, inhibition of biosynthetic and bioenergetic functions of the mitochondria can sensitize resistant cells to cyst(e)inase treatment. Alternately, inhibiting other antioxidant defense mechanisms, which is required to detoxify ROS produced by the ETC, greatly synergizes with GSH-depletion by cyst(e)inase with the most striking combinatorial effect and high translational potential provided by auranofin, a specific inhibitor of thioredoxin reductase and an FDA-approved drug for rheumatoid arthritis. This is illustrated in **(Figure 6.3 a**). While concurrently inhibiting the GSH and thioredoxin antioxidant systems is already known to produce synergistic cell killing of cancer cells *in vitro*[89,91], using BSO and auranofin to achieve this end *in vivo* might not be an effective therapeutic strategy[91]. Our current data demonstrate that co-administration of cyst(e)inase and auranofin can induce oxidative stress in multiple pancreatic cancer cells *in vitro* as well as *in vivo*, and has a favorable safety profile to justify further clinical evaluation. Furthermore, three-way combinations featuring cyst(e)inase, auranofin and additionally either BSO or the approved drug tigecycline produces synergistic inhibition of cell survival *in vitro* when compared to either agent alone or two-way combinations (**Figure 6.3 b**). It remains to be seen whether this synergy can be translated to mouse models without significant toxicity.

Chapter 7: Concluding Remarks

Cancer cells channel available nutrients in the serum such as glucose, glutamine and amino acids into distinct metabolic routes to support a rampant, proliferative program. Their biosynthetic and bioenergetic requirements are vastly different from non-proliferating, differentiated tissue, which leads to their exquisite dependence on certain nutrients. This differential requirement in cancer versus normal cells makes depletion of specific nutrients an exciting therapeutic approach. Under the umbrella of this strategy, amino acid depletion is a clinically tested modality as demonstrated by the successful use of the asparagine-depleting enzyme, asparaginase, as part of a combination therapy against pediatric acute lymphoblastic leukemia (ALL). However, the bacterial origin of this enzyme makes it very immunogenic, which leads to a panoply of side effects[92].

A superior approach is to use a human enzyme that is genetically engineered to degrade specific nutrients, which brings us to cyst(e)inase. This enzyme is generated via substitutions of just two amino acid residues in the human cystathionine-γ-lyase (CGL), which imparts unto the new enzyme an ability to degrade extracellular L-Cys and CSSC (collectively referred to as cyst(e)ine). Depletion of extracellular cyst(e)ine provides a wide enough therapeutic window due to cancer cells' increased demand for L-Cys that is not sufficed by intracellular synthesis and hence necessitates import from the extracellular space. This is demonstrated by the ability of cyst(e)inase to mediate growth inhibition of multiple tumor types. Furthermore, its remarkable safety profile evident in the absence of any significant toxicity even with treatment for over 5 months speaks volumes of its high translational potential[58].

Extending this exploratory work into the pancreatic cancer model, we discovered that a subset of pancreatic cancer cells was able to maintain survival during cyst(e)inase

treatment. We demonstrated that a cell's ability to evade the cytotoxic effects of cyst(e)ine depletion is correlated with its ability to maintain mitochondrial fitness. However, this is also a double-edged sword for the cell because a functional electron transport chain, the major producer of cellular ROS, demands an arsenal of antioxidants to combat potential oxidative stress. Consequently, the thioredoxin antioxidant system becomes a liability for resistant cells during cyst(e)ine starvation, which forms the basis of synergy achieved by combining cyst(e)inase with auranofin, an inhibitor of thioredoxin reductase.

There are several important translational implications of our findings. Clinical precedence with monotherapy in pancreatic cancer taken together with our results point towards the fact that cyst(e)inase is unlikely to prove efficacious as a single-agent, especially considering the fact that most pancreatic tumors requiring chemotherapy are advanced and harbor multiple genetic alterations that impart chemotherapeutic resistance. Here, we have identified the thioredoxin system as a synthetic lethal target with cyst(e)inase, which can be exploited with auranofin combination therapy to treat pancreatic cancers with various genetic alterations. Notably, auranofin, an FDA-approved drug for the treatment of rheumatoid arthritis, produced no systemic toxicity when combined with cyst(e)inase providing a strong rationale for advancing this drug combination further down the clinical development pipeline. Future exploration into other resistance mechanisms and identification of additional liabilities can guide better combination therapy options. For example, our preliminary data shows that a triple combination treatment of cyst(e)inase, auranofin and either BSO or tigecycline has a greater effect in cell survival inhibition than two drug combinations, a finding that is sure to spark interest for elucidating the mechanistic underpinnings behind this observation and for *in vivo* validation.

However, investigating the clinical efficacy of such combinations requires the challenging task of having to strike a balance between multiple aspects of drug

development such as circulatory persistence of each drug, effective drug concentration within the tumor, off-target effects leading to systemic toxicity etc. For example, pancreatic tumors are known to have a highly desmoplastic and hypovascular microenvironment, which makes drug-delivery an arduous task. Concomitantly, combining gemcitabine with an inhibitor of the Hedgehog signaling pathway to deplete tumor-associated stromal tissue enhanced the anti-tumor effect of gemcitabine[93]. Since depletion of cyst(e)ine from the serum is how cyst(e)inase exerts its anti-tumor effect, the problem of drug-delivery is circumvented; however, other combinatorial agents have to pass through this extra layer of consideration. Similarly, drugs that have lower circulatory persistence due to increased renal filtration cannot reach the tumor site in effective concentrations to exert their effects. In one of our *in vivo* experiments, the batch of cyst(e)inase that we were using was incompletely PEGylated – a fact that we discovered retrospectively when that experiment did not work. Switching to a well PEGylated batch resolved this problem demonstrating the importance of avoiding immediate renal clearance for a drug's *in vivo* efficacy. Another obstacle is systemic toxicity, which has to be carefully monitored. The greatest increase in survival (11.1 months) in pancreatic cancer to date has been achieved by the combination regimen in FOLFIRINOX, but it is also associated with more toxic side-effects[94].

An important issue that remains to be explored is the role of the tumor microenvironment in this context, and how we can use that knowledge to our benefit. It has been recently shown that pancreatic stellate cells recycle their intracellular contents through autophagy and "feed" the resulting nutrients, most notably alanine, to pancreatic cancer cells to support their growth[95]. A strategy to inhibit this cross-talk will likely enhance the effects seen with our amino acid depleting approach. Investigating the immune aspects of the microenvironment will also open up avenues for potential combinations with cancer immunotherapy modalities. Proliferation of activated T cells is dependent on uptake

of exogenous cyst(e)ine, and the inhibition of T-cell mediated anti-tumor immunity observed in many cancer cells is thought be caused by the depletion of cyst(e)ine by myeloid-derived suppressor cells[96,97]. Significant immune defects were not seen even with long-term cyst(e)inase treatment[58], but still the questions of whether anti-tumor immunity is blocked to some extent by cyst(e)inase, and whether synergy can be achieved with concurrent immunotherapy are ones worth finding answers to.

References

1 Www.cancer.org. Cancer Facts and Figures. (2017).

2 Paulson, A. S., Tran Cao, H. S., Tempero, M. A. & Lowy, A. M. Therapeutic Advances in Pancreatic Cancer. *Gastroenterology* **144**, 1316-1326 (2013).

3 Ryan, D. P., Hong, T. S. & Bardeesy, N. Pancreatic adenocarcinoma. *The New England Journal of Medicine* **371**, 2140-2141 (2014).

4 Aguirre, A. J. *et al.* Activated Kras and Ink4a/Arf deficiency cooperate to produce metastatic pancreatic ductal adenocarcinoma. *Genes Dev* **17**, 3112-3126 (2003).

5 DeNicola, G. M. *et al.* Oncogene-induced Nrf2 transcription promotes ROS detoxification and tumorigenesis. *Nature* **475**, 106-109 (2011).

6 Ying, H. *et al.* Oncogenic Kras maintains pancreatic tumors through regulation of anabolic glucose metabolism. *Cell* **149**, 656-670 (2012).

7 Viale, A. *et al.* Oncogene ablation-resistant pancreatic cancer cells depend on mitochondrial function. *Nature* **514**, 628-632 (2014).

8 Muzumdar, M. D. *et al.* Survival of pancreatic cancer cells lacking KRAS function. *Nat Commun* **8**, 1090 (2017).

9 Vander Heiden, M. G., Cantley, L. C. & Thompson, C. B. Understanding the Warburg effect: the metabolic requirements of cell proliferation. *Science* **324**, 1029-1033 (2009).

10 Chantranupong, L., Wolfson, R. L. & Sabatini, D. M. Nutrient-sensing mechanisms across evolution. *Cell* **161**, 67-83 (2015).

11 Ward, P. S. & Thompson, C. B. Metabolic reprogramming: a cancer hallmark even warburg did not anticipate. *Cancer Cell* **21**, 297-308 (2012).

12 Boroughs, L. K. & DeBerardinis, R. J. Metabolic pathways promoting cancer cell survival and growth. *Nat. Cell Biol.* **17**, 351-359 (2015).

13 Possemato, R. *et al.* Functional genomics reveal that the serine synthesis pathway is essential in breast cancer. *Nature* **476**, 346-350 (2011).

14 DeNicola, G. M. *et al.* NRF2 regulates serine biosynthesis in non-small cell lung cancer. *Nat. Genet.* **47**, 1475-1481 (2015).

15 Locasale, J. W. *et al.* Phosphoglycerate dehydrogenase diverts glycolytic flux and contributes to oncogenesis. *Nat. Genet.* **43**, 869-874 (2011).

16 Anastasiou, D. *et al.* Pyruvate kinase M2 activators promote tetramer formation and suppress tumorigenesis. *Nat. Chem. Biol.* **8**, 839-847 (2012).

17 Weinhouse, S., Millington, R. H. & Wenner, C. E. Metabolism of neoplastic tissue. I. The oxidation of carbohydrate and fatty acids in transplanted tumors. *Cancer Res.* **11**, 845-850 (1951).

18 Wenner, C. E., Spirtes, M. A. & Weinhouse, S. Metabolism of neoplastic tissue. II. A survey of enzymes of the citric acid cycle in transplanted tumors. *Cancer Res.* **12**, 44-49 (1952).

19 Marin-Valencia, I. *et al.* Analysis of tumor metabolism reveals mitochondrial glucose oxidation in genetically diverse human glioblastomas in the mouse brain in vivo. *Cell Metab.* **15**, 827-837 (2012).

20 Hensley, C. T. *et al.* Metabolic Heterogeneity in Human Lung Tumors. *Cell* **164**, 681-694 (2016).

21 Faubert, B. *et al.* Lactate Metabolism in Human Lung Tumors. *Cell* **171**, 358-371 e359 (2017).

22 Deberardinis, R. J., Sayed, N., Ditsworth, D. & Thompson, C. B. Brick by brick: metabolism and tumor cell growth. *Curr. Opin. Genet. Dev.* **18**, 54-61 (2008).

23 Svensson, R. U. *et al.* Inhibition of acetyl-CoA carboxylase suppresses fatty acid synthesis and tumor growth of non-small-cell lung cancer in preclinical models. *Nat. Med.* **22**, 1108-1119 (2016).

24 Hatzivassiliou, G. *et al.* ATP citrate lyase inhibition can suppress tumor cell growth. *Cancer Cell* **8**, 311-321 (2005).

25 Birsoy, K. *et al.* An Essential Role of the Mitochondrial Electron Transport Chain in Cell Proliferation Is to Enable Aspartate Synthesis. *Cell* **162**, 540-551 (2015).

26 Sullivan, L. B. *et al.* Supporting Aspartate Biosynthesis Is an Essential Function of Respiration in Proliferating Cells. *Cell* **162**, 552-563 (2015).

27 DeBerardinis, R. J. *et al.* Beyond aerobic glycolysis: transformed cells can engage in glutamine metabolism that exceeds the requirement for protein and nucleotide synthesis. *Proc. Natl. Acad. Sci. U. S. A.* **104**, 19345-19350 (2007).

28 Cetinbas, N. M. *et al.* Glucose-dependent anaplerosis in cancer cells is required for cellular redox balance in the absence of glutamine. *Sci. Rep.* **6**, 32606 (2016).

29 Cheng, T. *et al.* Pyruvate carboxylase is required for glutamine-independent growth of tumor cells. *Proc. Natl. Acad. Sci. U. S. A.* **108**, 8674-8679 (2011).

30 Lussey-Lepoutre, C. *et al.* Loss of succinate dehydrogenase activity results in dependency on pyruvate carboxylation for cellular anabolism. *Nat Commun* **6**, 8784 (2015).

31 Cardaci, S. *et al.* Pyruvate carboxylation enables growth of SDH-deficient cells by supporting aspartate biosynthesis. *Nat. Cell Biol.* **17**, 1317-1326 (2015).

32 Mullen, A. R. *et al.* Reductive carboxylation supports growth in tumour cells with defective mitochondria. *Nature* **481**, 385-388 (2011).

33 Yang, S. *et al.* Pancreatic cancers require autophagy for tumor growth. *Genes Dev.* **25**, 717-729 (2011).

34 Buzzai, M. *et al.* The glucose dependence of Akt-transformed cells can be reversed by pharmacologic activation of fatty acid beta-oxidation. *Oncogene* **24**, 4165-4173 (2005).

35 Dibble, C. C. & Manning, B. D. Signal integration by mTORC1 coordinates nutrient input with biosynthetic output. *Nat. Cell Biol.* **15**, 555-564 (2013).

36 Ye, J. *et al.* GCN2 sustains mTORC1 suppression upon amino acid deprivation by inducing Sestrin2. *Genes Dev.* **29**, 2331-2336 (2015).

37 Li, F. *et al.* Myc stimulates nuclearly encoded mitochondrial genes and mitochondrial biogenesis. *Mol. Cell. Biol.* **25**, 6225-6234 (2005).

38 Wise, D. R. *et al.* Myc regulates a transcriptional program that stimulates mitochondrial glutaminolysis and leads to glutamine addiction. *Proc. Natl. Acad. Sci. U. S. A.* **105**, 18782-18787 (2008).

39 Fernandez, C. A., Des Rosiers, C., Previs, S. F., David, F. & Brunengraber, H. Correction of 13C mass isotopomer distributions for natural stable isotope abundance. *J Mass Spectrom* **31**, 255-262 (1996).

40 Yoo, H., Antoniewicz, M. R., Stephanopoulos, G. & Kelleher, J. K. Quantifying reductive carboxylation flux of glutamine to lipid in a brown adipocyte cell line. *J. Biol. Chem.* **283**, 20621-20627 (2008).

41 Brunengraber, H., Kelleher, J. K. & Des Rosiers, C. Applications of mass isotopomer analysis to nutrition research. *Annu Rev Nutr* **17**, 559-596 (1997).

42 Sullivan, L. B. & Chandel, N. S. Mitochondrial reactive oxygen species and cancer. *Cancer Metab* **2**, 17 (2014).

43 Martindale, J. L. & Holbrook, N. J. Cellular response to oxidative stress: signaling for suicide and survival. *The Journal of Cellular Physiology* **192**, 1-15 (2002).

44 Ostman, A., Frijhoff, J., Sandin, A. & Bohmer, F. D. Regulation of protein tyrosine phosphatases by reversible oxidation. *Journal of Biochemistry* **150**, 345-356 (2011).

45 Connor, K. M. *et al.* Mitochondrial H2O2 regulates the angiogenic phenotype via PTEN oxidation. *The Journal of Biological Chemistry* **280**, 16916-16924 (2005).

46 Weinberg, F. *et al.* Mitochondrial metabolism and ROS generation are essential for Kras-mediated tumorigenicity. *Proc Natl Acad Sci U S A* **107**, 8788-8793 (2010).

47 Son, J. *et al.* Glutamine supports pancreatic cancer growth through a KRAS-regulated metabolic pathway. *Nature* **496**, 101-105 (2013).

48 Yang, S. *et al.* Pancreatic cancers require autophagy for tumor growth. *Genes & Development* **25**, 717-729 (2011).

49 Sahu, R. P., Zhang, R., Batra, S., Shi, Y. & Srivastava, S. K. Benzyl isothiocyanate-mediated generation of reactive oxygen species causes cell cycle arrest and induces apoptosis via activation of MAPK in human pancreatic cancer cells. *Carcinogenesis* **30**, 1744-1753 (2009).

50 Raj, L. *et al.* Selective killing of cancer cells by a small molecule targeting the stress response to ROS. *Nature* **475**, 231-234 (2011).

51 Trachootham, D. *et al.* Selective killing of oncogenically transformed cells through a ROS-mediated mechanism by beta-phenylethyl isothiocyanate. *Cancer Cell* **10**, 241-252 (2006).

52 Jeanne, M. *et al.* PML/RARA oxidation and arsenic binding initiate the antileukemia response of As2O3. *Cancer Cell* **18**, 88-98 (2010).

53 Tai, D. J. *et al.* Changes in intracellular redox status influence multidrug resistance in gastric adenocarcinoma cells. *Experimental and Therapeutic Medicine* **4**, 291-296 (2012).

54 Stewart, D. J. Mechanisms of resistance to cisplatin and carboplatin. *Critical Reviews in Oncology/Hematology* **63**, 12-31 (2007).

55 Gorrini, C., Harris, I. S. & Mak, T. W. Modulation of oxidative stress as an anticancer strategy. *Nat Rev Drug Discov* **12**, 931-947 (2013).

56 Belalcazar, A. D., Ball, J. G., Frost, L. M., Valentovic, M. A. & Wilkinson, J. t. Transsulfuration Is a Significant Source of Sulfur for Glutathione Production in Human Mammary Epithelial Cells. *ISRN Biochemistry* **2013**, 637897 (2014).

57 Conrad, M. & Sato, H. The oxidative stress-inducible cystine/glutamate antiporter, system x (c) (-) : cystine supplier and beyond. *Amino Acids* **42**, 231-246 (2012).

58 Cramer, S. L. *et al.* Systemic depletion of L-cyst(e)ine with cyst(e)inase increases reactive oxygen species and suppresses tumor growth. *Nat. Med.* **23**, 120-127 (2017).

59 Valsecchi, M. E., Diaz-Canton, E., de la Vega, M. & Littman, S. J. Recent treatment advances and novel therapies in pancreas cancer: a review. *J. Gastrointest. Cancer* **45**, 190-201 (2014).

60 Frese, K. K. *et al.* nab-Paclitaxel potentiates gemcitabine activity by reducing cytidine deaminase levels in a mouse model of pancreatic cancer. *Cancer Discov.* **2**, 260-269 (2012).

61 Von Hoff, D. D. *et al.* Increased survival in pancreatic cancer with nab-paclitaxel plus gemcitabine. *N. Engl. J. Med.* **369**, 1691-1703 (2013).

62 Conroy, T. *et al.* FOLFIRINOX versus Gemcitabine for Metastatic Pancreatic Cancer. *New England Journal of Medicine* **364**, 1817-1825 (2011).

63 Chou, T. C. & Talalay, P. Quantitative analysis of dose-effect relationships: the combined effects of multiple drugs or enzyme inhibitors. *Adv. Enzyme Regul.* **22**, 27-55 (1984).

64 Chou, T. C. Drug combination studies and their synergy quantification using the Chou-Talalay method. *Cancer Res.* **70**, 440-446 (2010).

65 Zhao, L., Wientjes, M. G. & Au, J. L. Evaluation of combination chemotherapy: integration of nonlinear regression, curve shift, isobologram, and combination index analyses. *Clin. Cancer Res.* **10**, 7994-8004 (2004).

66 Zhao, W. *et al.* A New Bliss Independence Model to Analyze Drug Combination Data. *J Biomol Screen* **19**, 817-821 (2014).

67 Lodi, A. *et al.* Combinatorial treatment with natural compounds in prostate cancer inhibits prostate tumor growth and leads to key modulations of cancer cell metabolism. *NPJ Precis Oncol* **1** (2017).

68 Boussemart, L. *et al.* eIF4F is a nexus of resistance to anti-BRAF and anti-MEK cancer therapies. *Nature* **513**, 105-109 (2014).

69 Ip, W. K. E., Hoshi, N., Shouval, D. S., Snapper, S. & Medzhitov, R. Anti-inflammatory effect of IL-10 mediated by metabolic reprogramming of macrophages. *Science* **356**, 513-519 (2017).

70 Sahu, R. P., Zhang, R., Batra, S., Shi, Y. & Srivastava, S. K. Benzyl isothiocyanate-mediated generation of reactive oxygen species causes cell cycle arrest and induces apoptosis via activation of MAPK in human pancreatic cancer cells. *Carcinogenesis* **30**, 1744-1753 (2009).

71 Guo, Z., Kozlov, S., Lavin, M. F., Person, M. D. & Paull, T. T. ATM activation by oxidative stress. *Science* **330**, 517-521 (2010).

72 Koppenol, W. H., Bounds, P. L. & Dang, C. V. Otto Warburg's contributions to current concepts of cancer metabolism. *Nat. Rev. Cancer* **11**, 325-337 (2011).

73 Birsoy, K. *et al.* Metabolic determinants of cancer cell sensitivity to glucose limitation and biguanides. *Nature* **508**, 108-112 (2014).

74 Jiang, L. *et al.* Reductive carboxylation supports redox homeostasis during anchorage-independent growth. *Nature* **532**, 255-258 (2016).

75 Ando, K. *et al.* A new APE1/Ref-1-dependent pathway leading to reduction of NF-kappaB and AP-1, and activation of their DNA-binding activity. *Nucleic Acids Res.* **36**, 4327-4336 (2008).

76 Hanigan, M. H. & Ricketts, W. A. Extracellular glutathione is a source of cysteine for cells that express gamma-glutamyl transpeptidase. *Biochemistry* **32**, 6302-6306 (1993).

77 Dringen, R., Kranich, O., Loschmann, P. A. & Hamprecht, B. Use of dipeptides for the synthesis of glutathione by astroglia-rich primary cultures. *J. Neurochem.* **69**, 868-874 (1997).

78 Quinlan, C. L. *et al.* Mitochondrial complex II can generate reactive oxygen species at high rates in both the forward and reverse reactions. *J. Biol. Chem.* **287**, 27255-27264 (2012).

79 Ackrell, B. A. Cytopathies involving mitochondrial complex II. *Mol. Aspects Med.* **23**, 369-384 (2002).

80 Thorburn, D. R., Rahman, J. & Rahman, S. in *GeneReviews((R))* (eds M. P. Adam *et al.*) (1993).

81 Shen, F. *et al.* Efficacy and safety of tigecycline for the treatment of severe infectious diseases: an updated meta-analysis of RCTs. *Int. J. Infect. Dis.* **39**, 25-33 (2015).

82 Wheaton, W. W. *et al.* Metformin inhibits mitochondrial complex I of cancer cells to reduce tumorigenesis. *Elife* **3**, e02242 (2014).

83 Lo, M., Ling, V., Wang, Y. Z. & Gout, P. W. The xc- cystine/glutamate antiporter: a mediator of pancreatic cancer growth with a role in drug resistance. *Br. J. Cancer* **99**, 464-472 (2008).

84 Folda, A. *et al.* Mitochondrial Thioredoxin System as a Modulator of Cyclophilin D Redox State. *Sci. Rep.* **6**, 23071 (2016).

85 Yamamoto, A. *et al.* Bafilomycin A1 prevents maturation of autophagic vacuoles by inhibiting fusion between autophagosomes and lysosomes in rat hepatoma cell line, H-4-II-E cells. *Cell Struct. Funct.* **23**, 33-42 (1998).

86 Wang, L. *et al.* Ethaselen: a potent mammalian thioredoxin reductase 1 inhibitor and novel organoselenium anticancer agent. *Free Radic. Biol. Med.* **52**, 898-908 (2012).

87 Lu, J. *et al.* Inhibition of Mammalian thioredoxin reductase by some flavonoids: implications for myricetin and quercetin anticancer activity. *Cancer Res.* **66**, 4410-4418 (2006).

88 Fang, J., Lu, J. & Holmgren, A. Thioredoxin reductase is irreversibly modified by curcumin: a novel molecular mechanism for its anticancer activity. *J. Biol. Chem.* **280**, 25284-25290 (2005).

89 Harris, I. S. *et al.* Glutathione and thioredoxin antioxidant pathways synergize to drive cancer initiation and progression. *Cancer Cell* **27**, 211-222 (2015).

90 Guo, J. Y. *et al.* Activated Ras requires autophagy to maintain oxidative metabolism and tumorigenesis. *Genes Dev.* **25**, 460-470 (2011).

91 Fath, M. A., Ahmad, I. M., Smith, C. J., Spence, J. & Spitz, D. R. Enhancement of carboplatin-mediated lung cancer cell killing by simultaneous disruption of glutathione and thioredoxin metabolism. *Clin. Cancer Res.* **17**, 6206-6217 (2011).

92 Hijiya, N. & van der Sluis, I. M. Asparaginase-associated toxicity in children with acute lymphoblastic leukemia. *Leuk. Lymphoma* **57**, 748-757 (2016).

93 Olive, K. P. *et al.* Inhibition of Hedgehog signaling enhances delivery of chemotherapy in a mouse model of pancreatic cancer. *Science* **324**, 1457-1461 (2009).

94 Conroy, T. *et al.* FOLFIRINOX versus gemcitabine for metastatic pancreatic cancer. *N. Engl. J. Med.* **364**, 1817-1825 (2011).

95 Sousa, C. M. *et al.* Pancreatic stellate cells support tumour metabolism through autophagic alanine secretion. *Nature* **536**, 479-483 (2016).

96 Levring, T. B. *et al.* Activated human CD4+ T cells express transporters for both cysteine and cystine. *Sci. Rep.* **2**, 266 (2012).

97 Srivastava, M. K., Sinha, P., Clements, V. K., Rodriguez, P. & Ostrand-Rosenberg, S. Myeloid-derived suppressor cells inhibit T-cell activation by depleting cystine and cysteine. *Cancer Res.* **70**, 68-77 (2010).